Doctoral Dissertation (Censored)

博士論文（要約）

Mechanisms for the distinctive seasonality of the North Pacific transient eddy activity as revealed from comprehensive analysis with the Eulerian statistics and Lagrangian tracking method

（北太平洋に特徴的な移動性擾乱活動の季節進行のメカニズムに関するオイラー的統計とラグランジュ的トラッキング手法による包括的な解析）

A Dissertation Submitted for the Degree of Doctor of Philosophy

January 2020

令和 2 年 1 月博士（理学）申請

Department of Earth and Planetary Science, Graduate School of Science,

The University of Tokyo

東京大学大学院理学系研究科 地球惑星科学専攻

Satoru Okajima

岡島　悟

Abstract

Extratropical transient eddies including migratory cyclones and anticyclones play an important role in our life, as they cause day-to-day weather phenomena. Extratropical cyclones, if intensified, give rise to many natural disasters, which potentially have massive socioeconomic impacts. Over decades, midlatitude stormtracks, where cyclone activity is particularly high, have been intensively investigated. Specifically, Eulerian statistics have enabled us to conduct quantitative diagnosis and analysis especially of eddy/mean-flow interactions, and objective Lagrangian tracking has revealed characteristics of cyclones and anticyclones separately. Although the Eulerian statistics and Lagrangian tracking are by nature intrinsically complementary, they have been applied separately in the previous studies or, at most, conducted just in parallel. Our understandings of extratropical stormtracks are thus still limited. As a typical example, stormtrack activity over the North Pacific exhibits a minimum in midwinter, since the westerly jet speed over the North Pacific clearly maximizes in midwinter. This counterintuitive phenomenon, which is inconsistent with the baroclinic instability theory, has been referred to as “midwinter minimum” and intensively investigated from various viewpoints. However, the mechanisms for the midwinter minimum have still many to be uncovered, and it remains one of the remaining difficult issues on midlatitude atmospheric and climate dynamics.

In the present study, we show the detailed seasonal evolution of climatological-mean Eulerian statistics and energetics of migratory eddies along the North Pacific stormtrack, for comprehensive investigation of the mechanisms for the midwinter minimum. We calculate the efficiency of each of the eddy energy conversion/generation terms, which is

independent of eddy amplitude for more straightforward analysis of the midwinter minimum. This study is the first to show that the net efficiency of eddy energy conversion/generation term is suppressed in midwinter mainly due to the baroclinic energy conversion via poleward eddy heat flux under reduced temperature fluctuations.

This study is also the first to develop a practical method to identify regions of cyclonic and anticyclonic vortices based on curvature vorticity, and to reconstruct Eulerian statistics from decomposed contributions from cyclonic and anticyclonic vortices. Westerly acceleration by cyclonic vortices is the strongest in midwinter and concentrated in the lower troposphere, acting to maintain the low-level eddy-driven jet and associated strong cyclonic shear on its northern flank. To the contrary, westerly acceleration by anticyclonic vortices is in deeper structure, acting to draw westerly momentum out of the merged climatological-mean jet in the upper troposphere. We then quantitatively investigate the energetics of migratory eddies along the North Pacific stormtrack from separated contributions from cyclonic and anticyclonic vortices. Total energy associated with anticyclonic vortices show more distinct midwinter suppression than its cyclonic counterpart. Consistently, midwinter suppression of efficiency of baroclinic energy conversion and its net efficiency are much clearer for anticyclonic vortices.

Surface cyclone density increases in midwinter and the region of high cyclone density extends southward in midwinter, while the latitude of maximum anticyclonic density migrates southward and anticyclonic density takes its minimum in midwinter over the North Pacific. The typical amplitude of cyclones is found slightly weaker in midwinter, whereas anticyclones tend to be maximized in midwinter. The cyclones are strongly

deformed under the background cyclonic shear. In the upper troposphere, the cyclonic eddies tend to be deformed in the direction of NE-SW to the south of the westerly jet, which is consistent with the southward wave-activity flux. Precipitation is large behind the anticyclonic center and poleward eddy heat flux is large both ahead of and behind the anticyclone center, reflecting the more wave-like structure. Anticyclones tend to tilt northwestward strongly with height.

A method to define the shape of vertically tilted eddy vortices is developed for the first time by combining surface Lagrangian tracking and vortex identification with curvature. High probability of cyclonic domain is in a deep profile to the north of the jet axis and is maximized in midwinter. High probability of anticyclonic domains is in a shallower structure to the south of the jet axis, with a midwinter minimum. Anticyclonic eddies play a more important role in forming the midwinter minimum of total climatological-mean strongly reinforce the lower-tropospheric jet and the associated strong cyclonic shear on its northern flank, while anticyclones act to draw westerly momentum out of the climatological-mean merged jet and to expand the westerly jet poleward in the upper troposphere. Analysis of energetics shows anticyclones show their more distinct midwinter minimum in total energy. The efficiency of the net energy conversion/generation for anticyclonic eddies throughout the winter. “Typical” energy or efficiency is further calculated by dividing energy or efficiency by the probability of cyclones and anticyclones. Seasonal evolution of the total energy for cyclonic eddies shows a weak midwinter minimum, while its anticyclonic counterpart is clearly maximized in midwinter. The efficiency of baroclinic conversion for cyclonic eddies is slightly suppressed in midwinter

and thus leads to a midwinter minimum of the efficiency of the net energy conversion/generation (referred to as “net efficiency”). Conversely, the efficiency of baroclinic conversion for anticyclonic eddies clearly exhibits a single peak in early winter, which is reflected in the net efficiency.

Furthermore, long-term modulation of the midwinter minimum of the North Pacific stormtrack activity are investigated. As pointed out by a previous study, the transition between 1985/86 and 1986/87 is striking, after which the midwinter minimum signal has become much less distinct in the Eulerian statistics. The midwinter suppression of the net efficiency is less prominent in the recent period. A relationship between westerly jet speed and Eulerian statistics suggests that the suppression of stormtrack activity under the stronger jet is substantially weaker in the recent period, especially for cyclones. The modulations of midwinter suppression in cyclonic and anticyclonic Eulerian statistics can be interpreted in the framework of energetics. In addition, the modulations of the midwinter minimum in the energetics as the total Eulerian statistics are found to be contributed to by both cyclones and anticyclones.

We have proposed a novel framework for studying stormtrack activity in which eddy-mean flow interaction is investigated by separating contributions from cyclones and anticyclones. It has the potential to renew our basic knowledge about the interaction based on Eulerian statistics widely, because the Eulerian statistics is widely used to investigate atmospheric and climate dynamics. In addition, we have proposed perspicuous clues for solving a difficult problem, namely the midwinter minimum of the North Pacific stormtrack activity.

Contents

1. General introduction

1.1. Eulerian statistics of transient eddy activity

Transient eddies (migratory cyclones and anticyclones) interact with the climatological-mean state and low-frequency, quasi-stationary anomalies, in largely regulating daily weather in midlatitude. Those eddies successively move eastward through a given midlatitude location, accounting for a major fraction of high-frequency fluctuations of a given atmospheric variable at a fixed point. Landsberg et al. (1959) found a variability whose periods are between 5-7 days in addition to that between 15-25 days from temperature data at a particular station. Based on a 10-year atmospheric analysis data over the entire Northern Hemisphere, Blackmon (1976) decomposed the temporal variance of 500-hPa geopotential height over the extratropical Northern Hemisphere into that of high-pass, band-pass, and low-pass filtered components, whose periods are less than 2 days, 2-6.5 days, not less than 10 days, respectively. They suggested that the regions of large band-pass variance of 500-hPa height closely corresponds to those of frequent cyclonic paths over the North Atlantic and Pacific basins, thus referred to as "stormtracks" (Fig. 1.1). This close correspondence had been first pointed out by Sawyer (1970) with data over the North Atlantic for two years. Blackmon et al. (1977) further pointed out that the stormtracks are characterized by strong poleward eddy heat flux based on band-pass filtered fluctuations at 850-hPa, which is now commonly used as a measure of development of baroclinic eddies. Zonally-elongated regions of maximum poleward heat transport associated with high-frequency eddies are located over the North Pacific, North Atlantic, and South Indian Ocean (Fig. 1.2). They tend to coincide closely with the lower-tropospheric eddy-driven

westerly jets and regions of strong baroclinicity in the lower-troposphere, where there are major oceanic frontal zones (Nakamura et al. 2004).

Until today, many studies have investigated climatological-mean, interannual or longer-scale variability, and seasonal evolution of stormtrack activity based on similar techniques for calculating Eulerian statistics (*e.g.*, Chang et al. 2002). A temporal filter is commonly used to investigate the behavior of extratropical high-frequency variability (*e.g.*, Wallace et al. 1988). The use of Eulerian statistics makes it much easier to apply quantitative analyses and physical diagnostic tools. Based on the partitioning of energy reservoirs, Lorenz (1955) proposed a framework of energetics to evaluate the exchanges between kinetic and available potential energy and between zonally averaged and eddy components (Fig. 1.3). Eulerian statistics are compatible with the analysis of energy conversions based on the "Lorenz energy cycle". For example, formation and maintenance mechanisms for the mean state and stormtrack activity can be examined through energy budget analysis (*e.g.*, Orlanski and Katzfey 1991; Chang et al. 2002), in the framework of Lorenz energy cycle. Eliassen-Palm (E-P) flux, which represents the propagation of a Rossby wave packet and translation of wave-activity pseudo-momentum toward the wave source, is also important for assessing the wave-mean flow interaction. It was extended to be able to be used in a three-dimensional space (Hoskins et al. 1983; Trenberth 1986; Plumb 1986), which can illustrate a zonal propagation of wave packets as well as zonal translation of pseudo-momentum.

Applying the Eulerian statistics, Nakamura et al. (2004) illustrated the maintenance mechanisms for the westerly jets and stormtracks by clearly separating eddy-driven,

subpolar jets, which correspond to the North Pacific shoulder seasons (autumn and spring) and the North Atlantic, and a stronger subtropical jet merged with a subpolar jet, which corresponds to the North Pacific midwinter (Fig. 1.4). In the former situation, stormtrack is anchored along the subarctic frontal zone (SAFZ) from the lower- to upper-troposphere. Transient eddies transport westerly momentum poleward and downward from the subtropical jet to maintain the deep eddy-driven jet. In the latter situation, by contrast, the upper-tropospheric stormtrack is trapped around the subtropical jet, while the lower-tropospheric stormtrack is located around the oceanic frontal zone. Transport of westerly momentum from the subtropical jet by transient eddies is relatively weak, and the eddy-driven jet is merged with the subtropical jet. They indicated that the structure and characteristics of the westerly jet have a close relationship with transient eddy activity.

As mentioned above, the Eulerian statistics have an advantage in conducting quantitative diagnosis and analysis. Note that the Eulerian statistics utilize gridded atmospheric data, including operational analysis and reanalysis data, which have been available since the mid-1970s. The Eulerian statistics are now widely used for analysis of numerical model outputs. However, it assumes a linearity of the variability and cannot target individual cyclones and anticyclones separately.

Figure 1.1

Map of wintertime RMS of bandpass-filtered geopotential height at 500-hPa, whose periods are between 2.5 and 6 days. Adopted from Blackmon (1976).

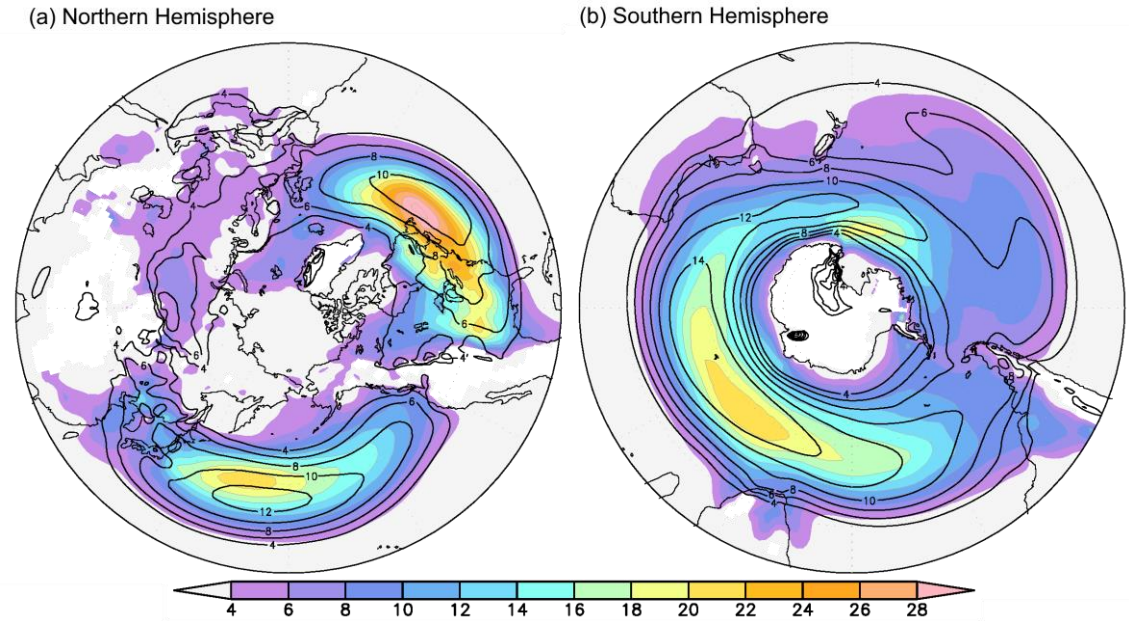

Figure 1.2

(a) Northern Hemispheric climatological-mean wintertime (DJF) poleward heat transport (color, m K/s) associated with high-frequency eddy component (deviation from lowpass filtered field with 8-day cutoff period), based on JRA-55 for 1958-2016. Contours denote climatological-mean U850 (m/s). (b) Same as in (a), but for the Southern Hemisphere in austral winter (JJA).

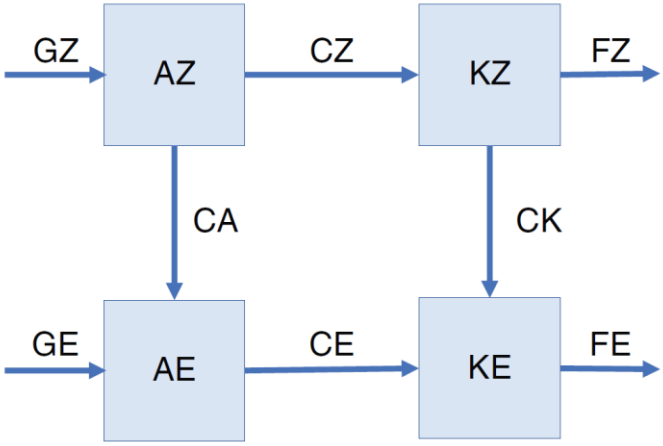

Figure 1.3

Schematic of Lorenz energy cycle. AZ: zonal mean available potential energy; AE: eddy available potential energy; KZ: zonal mean kinetic energy; KE: eddy kinetic energy. The generation, conversion, and dissipation terms are shown as G*, C*, and F*, respectively (where * is either Z or E). Adopted from Read et al. (2018).

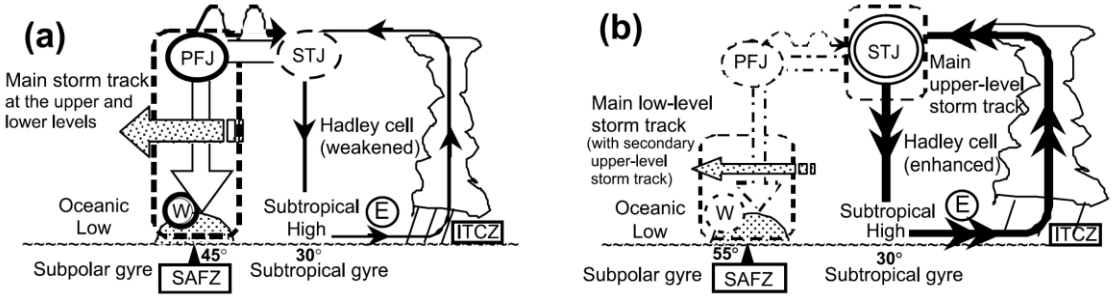

Figure 1.4

Schematics of different types of tropospheric general circulation over an ocean basin. (a) When a subtropical jet (STJ) is weak, the main storm track (thick dashed line) forms over a surface baroclinic zone (stippled at ~45° lat.) anchored by a subarctic frontal zone (SAFZ), as in the summertime SH, the North Atlantic or the North Pacific (in spring and fall). Wave-activity dispersion to the STJ (wavy arrow) leads to the formation of a deep polar-front jet (PFJ) above the SAFZ. Eddy downward transport (open arrow) of the mean-flow westerly momentum maintains a surface westerly jet (circled W) along the SAFZ. (b) When a STJ intensifies as in the wintertime South Pacific, the jet traps most of the upper-level eddy activity. Thus, the main branch of the upper-level storm track forms along the STJ with suppressed baroclinic eddy growth below, while the low-level storm track forms along a weak PFJ above a baroclinic zone anchored by the SAFZ. Adopted from Nakamura et al. (2004).

1.2. Lagrangian tracking of migratory cyclones and anticyclones

Extratropical transient eddies are a rudimentary component in meteorology and play an important role in maintaining the global energy budget. They are shaping day-to-day weather phenomena in the extratropics, which is directly related to our water supply. Extratropical cyclones, if intensified, cause many natural disasters in the extratropics, which have a massive socioeconomic impact throughout the world. Their occurrence and intensities are quite relevant to climate dynamics (*e.g.*, Hurrell 1995; Rogers 1997) and regional extreme weather events (*e.g.*, Catto and Pfahl 2013; Pfahl et al. 2014).

For more than a century, cyclone paths and intensities have been examined through tracking technique. In the late 19th century, typical paths of storms were already partly known in the Euro-Atlantic sector (*e.g.*, Hinman 1888). Then until the late 20th century, cyclonic frequency has been examined based on surface weather charts (*e.g.*, Klein 1958; Whittaker and Horn 1984), to reveal that cyclone frequency was particularly high over the North Pacific and North Atlantic (and Mediterranean Sea) (Fig. 1.5), which shows qualitative correspondence with the major stormtracks based on the Eulerian eddy statistics. However, the tracking technique is inherently subject to arbitrariness. With the development of (re-) analysis data, methods have been proposed to identify centers of cyclones and anticyclones more objectively based on gridded data (*e.g.*, Parker et al. 1989; Bell and Bosart 1989; Murray and Simmonds 1991; Hodges 1994, 1995). Until today, many studies have utilized various tracking algorithms (as reviewed by Ulbrich et al. 2009, for example). They identify and track centers of cyclones or anticyclones based typically

on fields of sea-level pressure (SLP) or low-level vorticity, which is referred to as "Lagrangian" tracking in the present study. Those Lagrangian tracking algorithms enable us to analyze individual transient eddies and concomitant phenomena directly, including winds, temperature and precipitation. Based on identified low-level cyclonic centers, composited structures of cyclones have been investigated by using atmospheric reanalysis data (*e.g.*, Manobianco 1989; Wang and Rogers 2001) and output of a GCM experiment (*e.g.*, Catto et al. 2010). Compared to the Eulerian statistics, however, Lagrangian tracking is not as suited for a quantitative diagnosis or dynamical diagnosis of eddy/mean-flow interaction.

It is apparently straightforward to track extratropical cyclones and anticyclones, but it is indeed challenging. There is no "definitive" version of Lagrangian tracking algorithm, because individual cyclones and anticyclones differ substantially in their shapes and structures. Neu et al. (2013) compared 15 different algorithms for cyclone tracking based on several variables in the same input data for the same time period. Despite a qualitative agreement among the obtained distributions of the number of cyclones, differences in the absolute number of cyclones are large among the methods.

Through a Lagrangian tracking, Hoskins and Hodges (2002) found that distributions of cyclone and anticyclone densities differ over the North Pacific in winter; the former is highest to the west of Japan, while the latter is high zonally around 30°N (Fig. 1.6). Later on, however, most of the tracking studies focused only on cyclones. Few studies conducted anticyclone tracking (*e.g.*, Favre and Gershunov 2006; Kravstov et al. 2015; Wernli and Papritz 2018), but they did not focus on the relationship of the obtained anticyclone tracks

with the midlatitude stormtrack activity identified as the Eulerian eddy statistics. Wallace et al. (1988) pointed out that variance maxima as Eulerian eddy statistics are exclusively associated with cyclone tracks and thus anticyclone tracks may be somehow irrelevant. Still, the role of migratory anticyclones in forming the North Pacific stormtrack or other major stormtracks has yet to be uncovered.

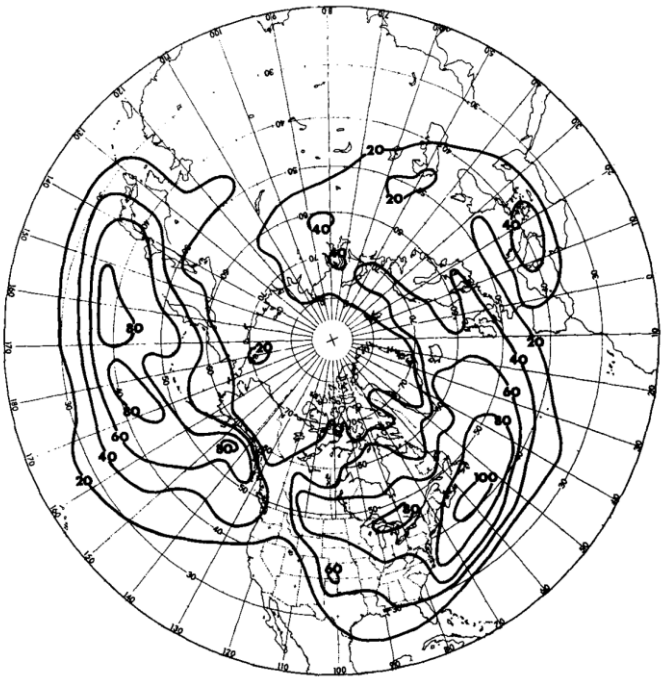

Figure 1.5

Climatological cyclone frequency for Januarys in the period of 1958-1977. Numbers indicate cyclone passages during the 20 years on 5° latitude-longitude grid. Adopted from Whittaker and Horn (1984).

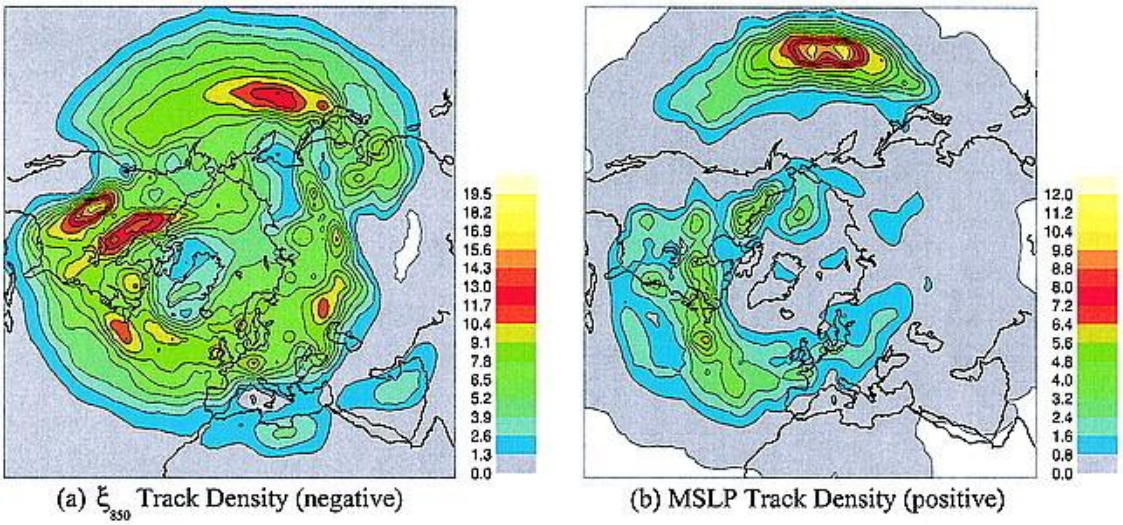

Figure 1.6

Wintertime track densities of (a) cyclones based on local maxima of 850-hPa relative vorticity and (b) anticyclones based on local maxima of SLP. The density statistics are subsequently scaled to number densities per month within a unit area equivalent to a 5° spherical cap (~10^6 km^2). Adopted from Hoskins and Hodges (2002).

1.3. Seasonality of transient eddy activity in the North Pacific

In the theory of baroclinic instability, the stronger vertical shear of the zonal wind speed (equivalent to meridional temperature gradient through the thermal wind balance) is, the larger the growth rate of eddies ($\sigma = 0.31\frac{f}{N}\frac{dU}{dz}$; Eady 1949) is. Consistently, the North Atlantic stormtrack activity measured by RMS of the band-pass filtered upper-tropospheric geopotential height fluctuations is strongest in midwinter, when the upper-tropospheric westerly jet speed is maximized (Fig. 1.7b). To the contrary, the corresponding North Pacific stormtrack activity has its minimum in midwinter (Nakamura 1992; Fig.1.7a). It is inconsistent with the baroclinic instability theory, since the westerly jet speed over the North Pacific is clearly maximized in midwinter.

This counterintuitive phenomenon is referred to as “midwinter minimum” or “midwinter suppression” of the North Pacific stormtrack activity, and it has long been investigated from various viewpoints. Nakamura (1992) and Nakamura et al. (2002) argued that an excessive propagation speed of baroclinic eddies inhibits the development of eddies by shortening the residence time over the baroclinic zone. The possible effect of the strong lateral hear of the extremely strong westerly jet in midwinter on suppressed growth rate of eddies was suggested by Harnik and Chang (2004) and Deng and Mak (2005). It is related to the results obtained by James (1987), who showed that enhanced lateral shear of the westerly jet acts to suppress baroclinic eddy growth (so-called “barotropic governor effect”). Afargan and Kaspi (2017) observed a clear suppression of high-frequency eddy activity even over the North Atlantic when the westerly jet is particularly strong. A similar result was obtained for a southward-shifted jet regime over

the North Atlantic by Madonna et al. (2019). Nakamura and Sampe (2002) pointed out that upper-tropospheric eddies were trapped into southward and upward shifted westerly jet in midwinter to be separated from the surface baroclinic zone, which is unfavorable for effective baroclinic growth of eddies (Nakamura et al. 2004; Fig. 1.4a). It was suggested that difference in vertical structure of the westerly Pacific jet between stronger and more subtropical, "merged" jet in midwinter and weaker eddy-driven jet in fall and spring can be responsible for the midwinter minimum (Lachmy and Harnik 2014, 2016; Yuval et al. 2018; Yuval and Kaspi 2018). Based on an idealized zonally symmetric GCM, Novak et al (2020) emphasized the importance of the equatorward shift of the westerly jet in midwinter. Furthermore, effect of diabatic heating associated with low-clouds in the cold sector of cyclones was argued by Chang (2001) and Chang and Song (2006). Through a Lagrangian tracking, Penny et al. (2010) focused on the importance of upper-level cyclonic eddies propagating from the Asian Continent upstream of the stormtrack ("seeding effect"). They argued that a decrease in their number in midwinter is responsible for the midwinter minimum, although such a clear relationship was not found in an independent analysis by Chang and Guo (2012). Penny et al. (2013) argued that the discrepancies were partly due to a difference in a perspective concerning whether cold seasons are viewed as one large dataset or individually. Park et al. (2010) and Lee et al. (2013) suggested the potential importance of orography in the midwinter minimum.

Still, the mechanisms for the midwinter minimum have many to be uncovered and are under debate. It is one of the difficult issues remaining in extratropical atmospheric and climate dynamics. The midwinter minimum was successfully simulated in GCM

experiments (Christoph et al. 1997; Zhang and Held 1999), but detailed mechanisms were not revealed in those studies. Zhang and Held (1999) successively simulated the midwinter minimum in a stochastic linear stormtrack model, implying that it is mainly caused by linear dry dynamics. However, a similar effort by Whitaker and Sardeshmukh (1998) was not successful. Chang (2001) and Zhao and Liang (2019) examined the energetics of migratory eddies along the Pacific stormtrack in relation to the midwinter minimum. However, they evaluated only energy conversion/generation rates, which is dependent of eddy amplitude. Their findings are therefore insufficient for full consideration of the mechanisms for the suppressed eddy activity. Recently, Schemm and Schneider (2019) attempted to evaluate "efficiency" of some of the energetic terms, which is independent of eddy amplitude. Their energetics analysis is, however, not comprehensive enough. It is therefore needed to investigate the comprehensive energetics of eddies along the North Pacific stormtrack to clarify the mechanisms for the midwinter minimum.

Recently, Hoskins and Hodges (2019a, b) investigated seasonal evolution of the number and intensity of upper- and lower-tropospheric cyclones over the Northern Hemisphere. In the western North Pacific, both the number and intensity of upper-tropospheric cyclones tend to minimize in midwinter, while the number of lower-tropospheric cyclones peaks in midwinter but their intensity has a weak midwinter minimum. Schemm and Schneider (2018) examined a relationship among stormtrack activity, number, and lifetime of surface cyclones. They suggested that shorter lifetime of cyclones in midwinter can contribute to the midwinter minimum of Eulerian stormtrack activity. However, distributions of Lagrangian surface cyclone density and the Eulerian activity differ substantially; the

density is highest over the Gulf of Alaska whereas the latter activity is strongest in the zonal band at ~40°N. In addition, a potential contribution of anticyclones was not assessed in those studies.

Nakamura et al. (2002) pointed out that the midwinter minimum of the North Pacific stormtrack activity had been distinct in the early to mid-1980s, but it has almost vanished afterward (Fig. 1.8). They argued that it occurred concomitantly with the decadal weakening of the surface Siberian High and Aleutian Low and the associated East Asian winter monsoon. The enhancement of the midwinter stormtrack activity occurred despite the reduced westerly jet intensity. This transition is also against the linear theory of baroclinic instability as the climatological midwinter minimum (Nakamura 1992). They suggested that eddies have changed their structure in the later period so as to be more efficient in converting the mean-flow available potential energy into their kinetic energy for their growth. However, their analysis was based on a short data period to capture the robust characteristics of the decadal-scale stormtrack variability. There are still many to unveil about the long-term modulations.

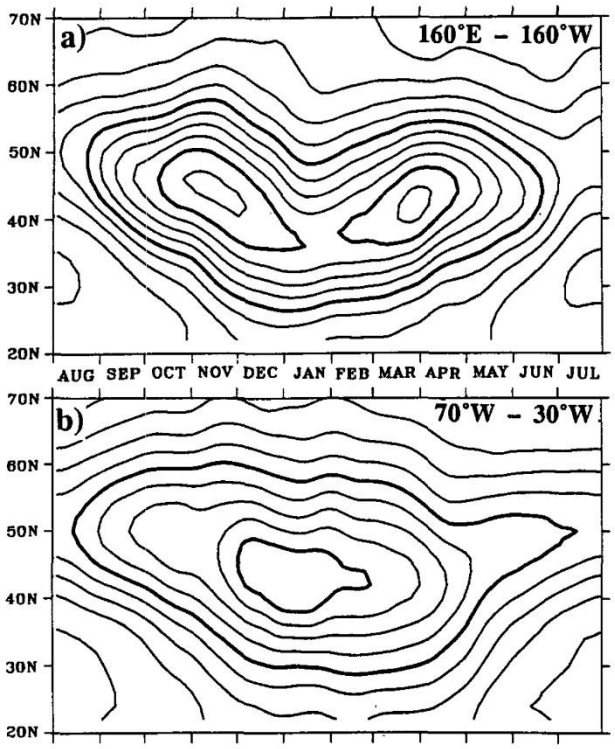

Figure 1.7

Latitude-season sections showing the seasonal march of baroclinic wave amplitude in Z250 averaged over the longitude intervals (a) 160°E-160°W and (b) 70°W-30°W. The plot is based on 31-day running-mean envelope function of 6-day highpass-filtered data. A binomial filter is applied twice along the time axis. Contour interval is 10m and heavy lines correspond to 80 and 120 m. Adopted from Nakamura (1992).

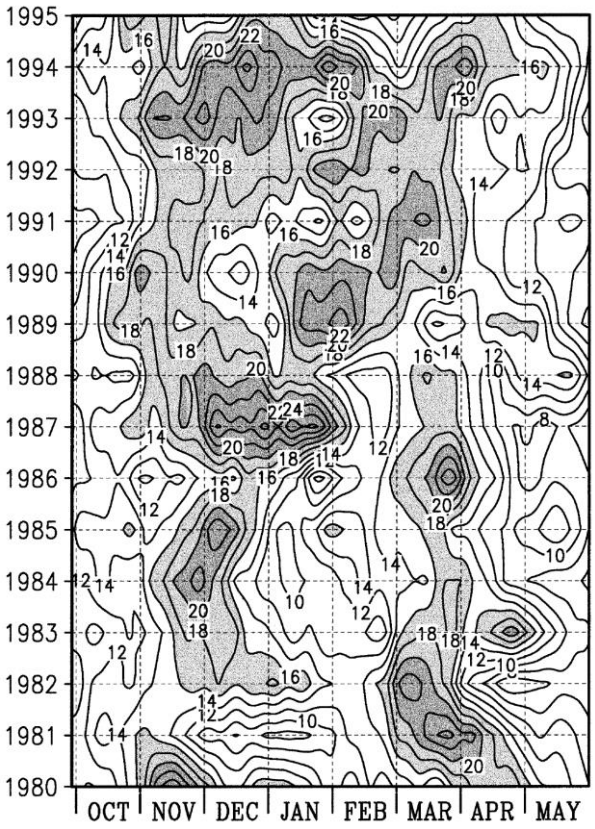

Figure 1.8

Year–month section showing interannual modulations in the seasonal march of the storm track activity over the NW Pacific. The activity is measured as the highpass-filtered poleward eddy heat flux at 850-hPa (K m/s), which has been sampled within a 108 latitudinal band centered at its maximum (*i.e.*, storm track axis) at each meridian in its daily 31-day running-mean field and then averaged in 140°E -180°. Each of the years along the ordinate corresponds to a particular winter season that starts in Oct of the previous year Adopted from Nakamura et al. (2002).

1.4. Purpose of this study

Over decades, a number of studies have intensively investigated the characteristics and dynamics of midlatitude stormtracks. However, our understandings of stormtracks are still limited. Eulerian statistics facilitate a quantitative diagnosis and analysis but cannot separate cyclones and anticyclones. Lagrangian tracking, by contrast, enables us to analyze them separately but is not suited for a quantitative analysis, especially of eddy/mean-flow interactions. Obviously, these two methods are intrinsically complementary, but they have been applied separately in most of the previous studies. Some studies conducted analyses of both Eulerian statistics and Lagrangian tracking, but just in parallel (Chang et al. 2002; Hoskins et al. 2019a, b). In fact, the region of maximum high-frequency Eulerian statistics and the cyclone tracks are not synonymous. Wallace et al. (1988) documented the behavior of high-frequency fluctuations in geopotential height and revealed that cyclones tend to move northeastward to the east of Japan, but not along the zonally-elongated "stormtrack" identified in Blackmon (1976). They mentioned that the term "*storm track*" used by Blackmon (1976) as a label of the Eulerian maxima can be misleading[1].

In the present study, we first investigate the comprehensive energetics of migratory eddies along the Pacific stormtrack to elucidate the mechanisms for the midwinter minimum. We evaluate and compare the efficiency of each term of energy conversion and generation terms. Then, analyses of Eulerian statistics and Lagrangian tracking are integrated. We propose a specific strategy to overcome the difficulties in the integration.

[1] However, the term "stormtrack" will be used in the remainder of this dissertation, since it is so entrenched that it makes the dissertation more complicated to replace the term. We will use the term with carefully recognizing what it means in a given context.

We focus on not only cyclones but also anticyclones. We propose a novel framework for studying stormtracks in which dynamics of eddy/mean-flow interactions are investigated with specific strategies to tackle the remaining difficult problem, that is the midwinter minimum of the North Pacific stormtrack activity, to offer several important new implications for future studies associated with stormtracks.

The dissertation is structured as follows. In Chapter 2, datasets and analysis methods used in this study, including the tracking algorithm of cyclones and anticyclones are described. In Chapter 3, seasonal evolutions of climatological-mean Eulerian statistics of the North Pacific stormtrack activity are investigated, including transient eddy feedback forcing onto the background westerlies, energetics, and their long-term modulations. In Chapter 4, a new method to separate cyclonic and anticyclonic vortices from gridded data is developed. Separated contributions of cyclone and anticyclone vortices to Eulerian statistics and feedback forcing onto climatological-mean westerly wind are described. In Chapter 5, results of Lagrangian tracking, including statistics of cyclone and anticyclone centers and composite maps, are discussed comprehensively. Then, Lagrangian tracking and Eulerian statistics are integrated for full, in-depth description of the seasonal evolution of climatological-mean Eulerian statistics of the North Pacific stormtrack activity based on the separated contributions from cyclones and anticyclones. Discussion and concluding remarks are given in Chapter 6, where implications of this study and a scope for future studies are mentioned for deepening our understanding of stormtracks.

2. Data and analysis methods

2.1. Data and temporal filter

In this study, 6-hourly atmospheric variables, including SLP and geopotential height, air temperature, wind velocity, and diabatic heating rates in the pressure coordinates, are obtained from the Japanese 55-year reanalysis (JRA-55) by the Japan Meteorological Agency (JMA) (Kobayashi et al. 2015, Harada et al. 2016) for the period 1958-2017. The JRA-55 is constructed with a four-dimensional variational data assimilation (4D-Var) system with TL319 horizontal resolution (equivalent to 55-km) and 60 vertical levels up to 0.1-hPa. Variables on pressure levels are available on 1.25°×1.25° grid. Diabatic heating rate is decomposed into five terms: parameterized convective precipitation, large-scale grid-scale precipitation, shortwave radiation, longwave radiation, and vertical diffusion. When diabatic heating associated only with precipitation is considered, we take a sum of the first two terms.

At a particular grid, fluctuation of a given variable with synoptic-scale transient eddies whose period is shorter than about a week has been extracted from the 6-hourly atmospheric reanalysis as its deviations from their low-pass-filtered fields with 8-day Lanczos filter (hereafter, primes denote local deviations from the climatological-mean unless otherwise specified). Local activity of those transient eddies or their fluxes is evaluated as the variance based on the sub-weekly fluctuations of meridional velocity or covariance representing poleward eddy heat flux corresponds to “stormtrack”, along which many transient eddies recurrently develop.

2.2. Analysis methods

a. Energetics

High eddy activity along stormtracks is likely to be maintained through energy conversion from the climatological-mean background state and/or energy generation through diabatic processes. To investigate the maintenance mechanisms for the stormtrack, local energy conversion/generation rates are calculated (Orlanski and Katzfey 1991; Chang et al. 2002). A schematic diagram of the energy budget concerning the climatological-mean background state and stormtrack is shown in Fig. 2.1, where eddy available potential energy (EAPE) and eddy kinetic energy (EKE) associated with synoptic-scale disturbances are defined as follows:

$$EAPE = \frac{R}{pS_p}\left(\frac{(T'^2)_C}{2}\right),\ EKE = \frac{(u'^2+v'^2)_C}{2}. \tag{2.1}$$

In Eq. (2.1), primes denote high-pass filtered fields and subscripts "c" the climatological-mean, and S_p ($\equiv -\overline{T}_c\,\partial \ln\overline{\theta}_c/\partial p$) a stability parameter, where overbars denote horizontally-averaged quantities over a specific domain. Furthermore, R signifies the gas constant for dry air, p pressure, T temperature, u zonal wind, and v meridional wind velocities. On calculating the horizontal average, grids below the Earth surface are masked out based on climatological-mean surface pressure, and the set of grid points used for horizontal averaging is set to be identical for the particular level at which S_p is calculated and the two adjacent levels, in order to minimize the effect of topography. In Fig. 2.1, *CK* denotes the barotropic energy conversion (or KE conversion), *CP* the baroclinic energy conversion (or APE conversion), *CQ* the APE generation through diabatic processes, and *ET* energy transfer from EAPE to EKE. Each of the energy conversion/generation terms is

expressed as follows:

$$CK = \frac{(v'^2 - u'^2)_C}{2}\left(\frac{du_c}{dx} - \frac{dv_c}{dy}\right) - (u'v')_C\left(\frac{du_c}{dy} + \frac{dv_c}{dx}\right) \quad (2.2a)$$

$$CP = \frac{R}{pS_p}\left(-(u'T')_C\frac{dT_c}{dx} - (v'T')_C\frac{dT_c}{dy}\right) \quad (2.2b)$$

$$CQ = \frac{R}{pS_p}(Q'T')_C \quad (2.2c)$$

$$ET = -\frac{R}{p}(\omega'T')_C, \quad (2.2d)$$

where Q denotes temperature tendency associated with diabatic processes and ω vertical motion.

These energy conversion/generation terms were integrated vertically from the surface to the 100-hPa level and then integrated horizontally within a specified domain. In this study, a central focus is the energetics of eddies along the North Pacific stormtrack, thus the region is [130°E-130°W, 20-65°N] unless otherwise specified. When the energetics within a local domain is discussed, energy inflow or outflow by energy fluxes through its lateral boundaries (*EF* in Fig. 2.1) is also estimated. The energy flux can be described as follows:

$$\mathbb{E} = \int_{p_s}^{p_{top}}\{(\Phi'\mathbb{v}')_C + (EAPE + EKE)\mathbb{v}_c\}\, dp, \quad (2.3)$$

where Φ is geopotential, p_s denotes surface pressure, and p_{top} is set to be 100-hPa.

For more quantitative discussion on the energetics based on Eqs. (2.1)-(2.3), "efficiency" of each of the conversion/generation and flux terms is evaluated by dividing it by the total energy associated with transient eddies (defined as the sum of EAPE and EKE):

$$\text{Efficiency} \equiv \frac{\text{<Energy conversion/generation term>}}{\text{<EAPE+EKE>}}. \quad (2.4)$$

This "conversion (or generation) efficiency" is evaluated in unit of [day^{-1}], and its

reciprocal gives a measure of how long it would take to replenish the total energy of the stormtrack sorely by a given conversion/generation process. Because the energy conversion/generation rates are dependent on eddy amplitude by definition, it is important to evaluate the conversion/generation as its efficiency, which is independent of amplitude of eddy amplitude, for the investigation of maintenance mechanisms for stormtracks.

b. Estimation of transient eddy feedback forcing

Feedback forcing exerted on quasi-steady background state from eddy along a stormtrack is estimated locally as a geopotential height tendency that could be induced through fluxes of heat and vorticity by transient eddies (Lau and Holopainen 1984; Nishii et al. 2009), as follows:

$$\frac{\partial \mathrm{z}}{\partial t} = \frac{1}{g}\left(\nabla^2 + f^2\frac{\partial}{\partial p}\left(\frac{1}{\sigma}\frac{\partial}{\partial p}\right)\right)^{-1} \cdot \left(-f\nabla\cdot(\mathbb{v}\zeta) + f^2\frac{\partial}{\partial p}\left(\frac{-\nabla\cdot(\mathbb{v}\theta)}{-\frac{\partial \Theta}{\partial p}}\right)\right)$$

$$\sigma = -\frac{\partial \Theta}{\partial p}\frac{R}{p}\left(\frac{p}{p_{00}}\right)^{R/c_p}. \qquad (2.5)$$

The feedback forcing by high-frequency transient eddies was estimated through the eddy fluxes as evaluated in a manner described above. The high-frequency transients are always exerting feedback forcing onto the background state in which they are embedded, and their feedback forcing must therefore be balanced with other processes in the climatological-mean state and low-frequency variability. Eddy feedback forcing as acceleration (or deceleration) of westerly wind is estimated by calculating westerly wind tendency based on the relationship of geostrophic wind. The forcing terms associated with $-f\nabla\cdot(\mathbb{v}\zeta)$

and $f^2\frac{\partial}{\partial p}\begin{pmatrix}\frac{-\nabla\cdot(\mathbb{v}\theta)}{\partial\Theta}\\ -\frac{\partial\Theta}{\partial p}\end{pmatrix}$ in Eq. (2.5) are referred to as "vorticity flux term" and "heat flux term", respectively.

c. Wave activity flux

We evaluate the stationary component of a particular expression of a wave-activity flux defined by Takaya and Nakamura (2001) in pressure coordinates. The wave-activity flux is defined as follows;

$$\mathbb{W} = \mathbb{W}_s + \mathbb{C}_U M$$

$$\mathbb{W}_s = \frac{1}{2|\bar{\mathbb{U}}|}\begin{pmatrix}\bar{U}\left(\psi_x'^2 - \psi'\psi_{xx}'\right) + \bar{V}\left(\psi_x'\psi_y' - \psi'\psi_{xy}'\right)\\ \bar{U}\left(\psi_x'\psi_y' - \psi'\psi_{xy}'\right) + \bar{V}\left(\psi_y'^2 - \psi'\psi_{yy}'\right)\\ \frac{f^2}{S^2}\left(\bar{U}\left(\psi_x'\psi_p' - \psi'\psi_{xp}'\right) + \bar{V}\left(\psi_y'\psi_p' - \psi'\psi_{yp}'\right)\right)\end{pmatrix} \quad (2.6)$$

where ψ indicates streamfunction, $\mathbb{U} = (U, V)$ horizontal wind vector, $\mathbb{C}_\mathrm{U}$ the phase speed projected onto the direction of $\mathbb{U}$, M the wave-activity pseudomomentum, and $S^2 = -\alpha\frac{\partial \ln\theta}{\partial p}$ the static stability parameter. In the equation, overbars and primes indicate basic state and perturbation quantities, respectively. The flux $\mathbb{W}$ is parallel to the local group velocity of stationary Rossby wave and independent of wave phase theoretically. The stationary component $\mathbb{W}_\mathrm{s}$ illustrates the propagation of wave packets relative to eastward-moving eddy centers with $\mathbb{C}_\mathrm{U}$ and is the same as defined for stationary Rossby waves by Takaya and Nakamura (1997). In other words, eastward $\mathbb{W}_\mathrm{s}$ illustrates downstream development of eddies.

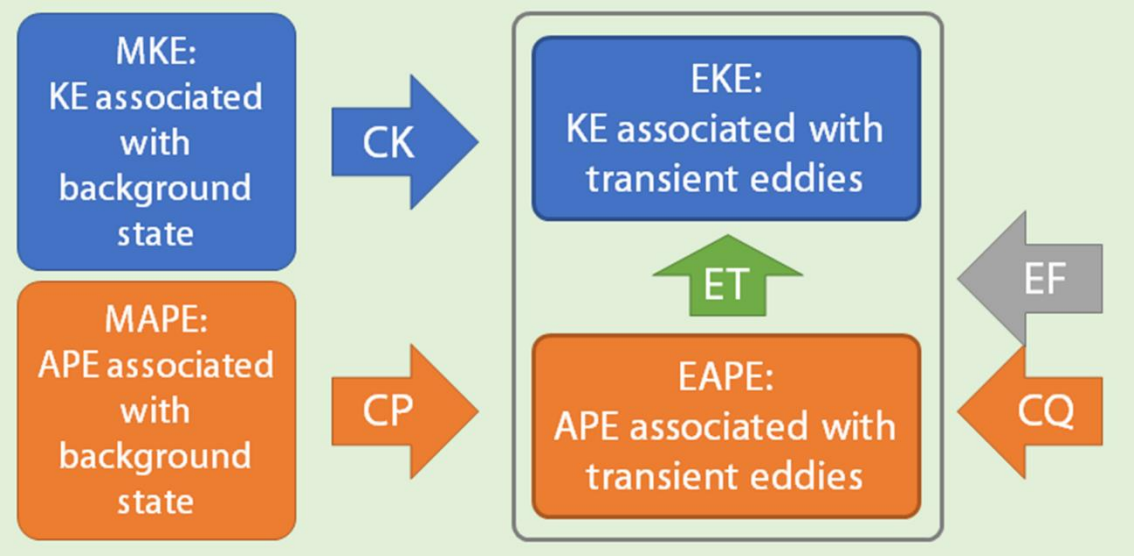

Figure 2.1

Schematic diagram of the energetics for eddies migrating along the climatological-mean westerlies and stormtracks. Orange arrows (CK) indicate conversion of eddy kinetic energy (EKE) into stormtrack, and blue arrows the conversion (CP) of eddy available potential energy (EAPE), and APE generation through diabatic processes (CQ). ET denotes energy transfer from EAPE to EKE, and EF denotes net energy influx through lateral boundaries.

2.3. Cyclone and anticyclone track identification algorithm

In this study, tracks of cyclone and anticyclone centers are objectively identified based on the reanalysis data. The procedure is the following.

a. Cyclone tracks

For tracking cyclones centers, SLP and the Laplacian of SLP (hereafter, ∇^2SLP) are utilized. Before the tracking starts, a Gaussian spatial filter whose half-amplitude length is 300km is applied to ∇^2SLP to obtain a smoother field. Grid points whose altitudes are higher than 1500m are not used for the tracking.

First, local minima of SLP are sought as candidates for cyclone centers, and among them only the SLP minimum with the lowest pressure in the vicinity of a 400km circle has been identified. The SLP minimum must accompany a local maximum of ∇^2SLP within 700km, which must be stronger than 80 Pa/(100km)^2. This condition is imposed to discard cyclones with not significant amplitudes.

Next, those SLP minima identified above are compiled as tracks. The nearest SLP minima at successive time steps are connected, only when the distance is not more than 800km. Any track must be not shorter than 4 time steps (24 hours) and must move at distance not less than 600km in their lifetime. A cyclone track must pass through a domain around the North Pacific stormtrack (100°E-120°W, 20-65°N).

b. *Anticyclone track*s

For anticyclone centers, only SLP is used because anticyclones are not likely to have

distinct ∇^2SLP minima around its center, reflecting the gradient wind balance that differs from that for cyclones. Local maxima of SLP are sought as candidates for anticyclone centers, after SLP has been horizontally smoothed with performing a 9-point horizontal smoothing (weight is 0.5 next to the center point and 0.3 at corners) eight times. Here, only a SLP maximum that is highest within a 400km circle around the maximum is identified as a surface anticyclonic center that must not lower than 990 hPa.

Similar to the case for cyclone centers, nearest SLP maxima identified above at successive time steps are connected. The distance must be not more than 1000km. Again, any track must be not shorter than 4 time steps (24 hours) and must move at distance not less than 600km in their lifetime. Any anticyclone track must pass through the domain around the North Pacific stormtrack (100°E-60°W, 20-65°N).

c. *Benchmark of the algorithm*

The criteria and parameters mentioned above have been chosen to identify features as cyclones and anticyclones represented on a surface weather map, taking the different characteristics between typical characteristics of cyclones and anticyclones into account. Indeed, identified cyclone/anticyclone centers are consistent with a SLP field in a snapshot (Fig. 2.2). Results shown in this study are qualitatively similar when longer thresholds for movement are imposed (*e.g.*, 1000km).

The climatological-mean wintertime densities of cyclones and anticyclones are shown in Fig. 2.3. Cyclone density is large over the north of approximately 30°N over the North Pacific, associated with the climatological-mean Aleutian Low. A narrow band of large

density is located along the south coast of Japan and extends northeastward, which is consistent with typical northeastward-moving cyclones along the southern coast of Japan in a synoptic viewpoint. To the contrary, anticyclone density has a zonally-elongated maximum along ~30°N, which is close to the climatological subtropical high pressure belt. Anticyclones tend to move southeastward around Japan. Detailed results from the tracking algorithm will be shown in Chapter 5.

The identification algorithm described above includes some degree of arbitrariness. It is therefore important to compare our results with those in previous studies. The cyclone density with our tracking algorithm is consistent with those obtained in the IMILAST project (Neu et al. 2013), especially with algorithms using SLP and vorticity (corresponding to ∇^2SLP) in its overall density values and horizontal distribution (three algorithms shown in Fig. 2.4). The anticyclonic density has much fewer previous references to be compared with, but it is consistent with the result in Hoskins and Hodges (2002).

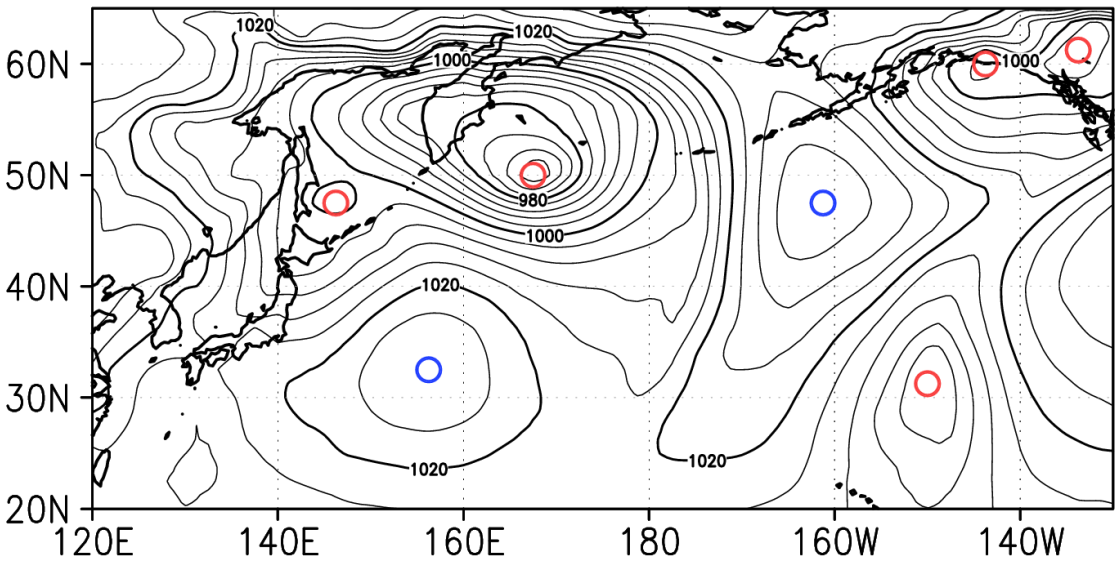

Figure 2.2

Snapshot of SLP (black contours, every 4hPa) and identified cyclone and anticyclone centers (red and blue open circles) at 00z31Dec1958.

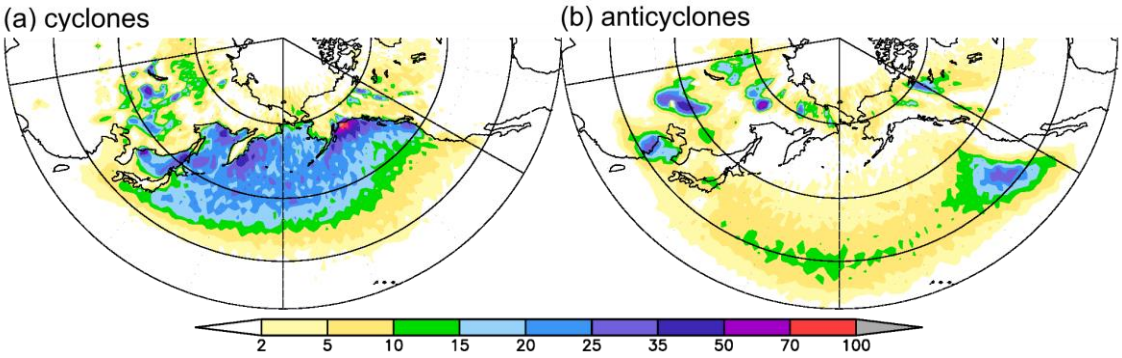

Figure 2.3

Wintertime (DJF) climatological-mean density of (a) cyclone and (b) anticyclone centers (%/(1000km)^2) based on the JRA-55 in 1988/89-2008/09. Unit is set to be the same in Neu et al. (2013). Meridians of 100°E and 120°W are highlighted, which indicate the western and eastern boundaries of the domain identified centers have to pass.

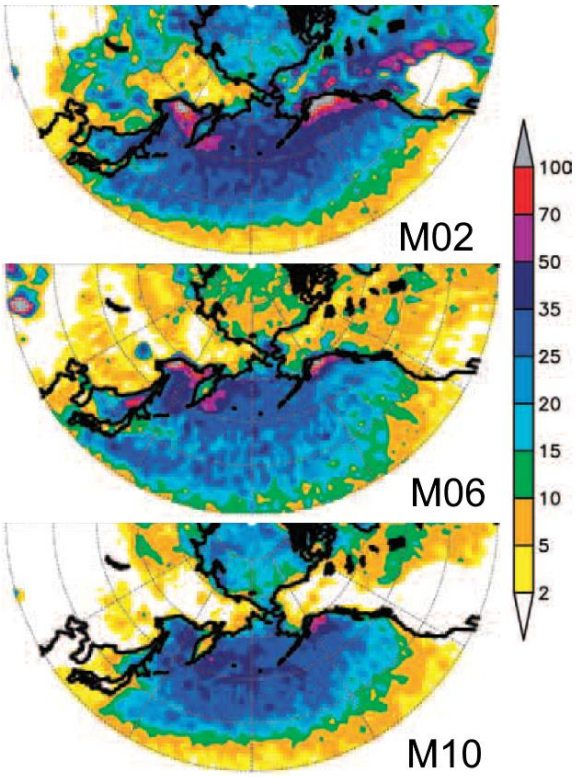

Figure 2.4

Wintertime (DJF) climatological-mean density of cyclone centers (%/(1000km)^2) adopted from Neu et al. (2013). Results are based on the ERA-Interim interpolated into a 1.5°×1.5° grid for Jan1989-Mar2009. Labels denote code numbers of algorithm used in Neu et al. (2013).

3. Eulerian eddy statistics for the North Pacific stormtrack

第 3 章

本章については、5 年以内に雑誌等で刊行予定のため、非公開。

4. Separating contributions from cyclonic and anticyclonic eddies to Eulerian statistics

第 4 章

本章については、5 年以内に雑誌等で

刊行予定のため、非公開。

5. Integration of Lagrangian tracking and Eulerian statistics

第 5 章

本章については、5 年以内に雑誌等で

刊行予定のため、非公開。

6. General discussions and conclusions

第 6 章

本章については、5 年以内に雑誌等で刊行予定のため、非公開。

Appendix A: Comparison of the energetics between different reanalysis datasets

In the present study, we have utilized the JRA-55 reanalysis. In Chapter 3, we have investigated the detailed energetics for the North Pacific stormtrack. Here, our result is compared with the energetics based on the ERA-Interim data produced by the European Centre for Medium Range Weather Forecasts (ECMWF) (Dee et al. 2011). Climatological mean is calculated for the period of 1979/80-2016/17, for which the ERA-Interim data is available. No diabatic heating rate is available for the ERA-Interim, and therefore CQ is not calculated in the following.

The results of energetics based on ERA-Interim are shown in Fig. A.1. Climatological-mean amplitudes of EKE and EAPE are quite similar to those based on JRA-55 (Fig. 3.17a). Their seasonality also resembles that in Chapter 3, featuring their early-winter peak. Their midwinter suppression is somewhat weaker in ERA-Interim, presumably because ERA-Interim is available for only a small fraction of the earlier period of 1958/19 through 1985/86, when the midwinter suppression was more distinct (Section 3.3). Efficiencies of CP, CK, ET, and EF reproduce their counterparts with the JRA-55: early-winter peaks of CP and ET, and more destructive CK and EF in midwinter. Their efficiencies, which is calculated by dividing the energy terms by total energy associated with transient eddies, are also quite similar to those with the JRA-55 (Fig. 3.17c). CP is the most efficient process for the maintenance of the North Pacific stormtrack, while CK is weakly destructive. As shown in Fig. A.2, seasonal evolutions of the zonal and meridional contributions to CK and CP obtained aby JRA-55 are also reproduced with ERA-Interim, including the

dominance of meridional component of CP (Fig. 3.18). It is confirmed that the results of the energetics for migratory eddies along the North Pacific stormtrack is not sensitive to a particular reanalysis data used.

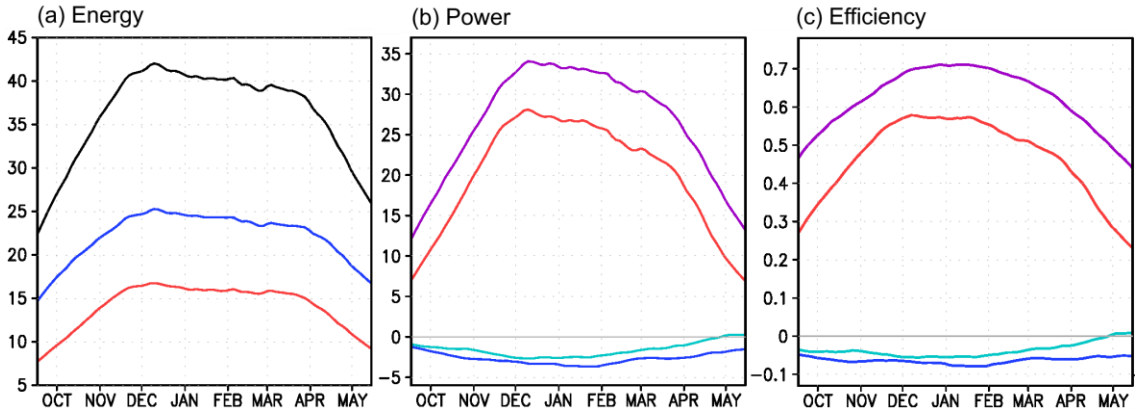

Figure A.1

(a) Climatological-mean seasonal evolution of EKE (blue), EAPE (red), and EKE+EAPE (black) integrated three-dimensionally over the North Pacific (10^{19}J) based on ERA-Interim. (b) Same as in (a), but for power of CK (blue), CP (red), ET (purple), and EF (light blue). Units are 10^{14}W. (c) Same as in (b), but for efficiency of CK (blue), CP (red), ET (purple), and EF (light blue). Units are day^{-1}.

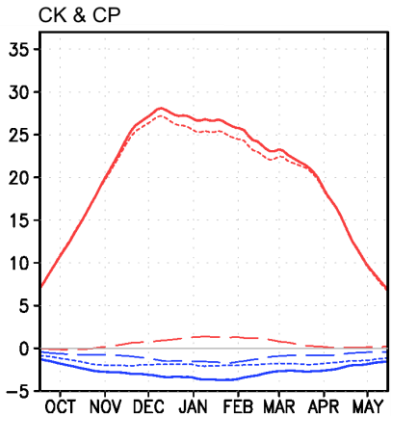

Figure A.2

Same as in Fig. A.1b, but for zonal (dashed lines) and meridional (dotted lines) contributions, in addition to total (solid lines) CK (blue) and CP (red).

Appendix B: Sensitivity of separated Eulerian statistics to temporal filtering

In Chapter 5, we have investigated the Eulerian statistics separately for cyclonic and anticyclonic eddies based on a Lanczos filter with cutoff period of 8 days. The filter is used to extract sub-weekly fluctuations associated with migratory eddies for the Eulerian statistics. To assess the sensitivity of the energetics to the cutoff period of the temporal filter, here we compare results for eddy components extracted as deviations from 31-day running mean.

Figure A.3 shows climatological-mean V'V'300 separated into contributions from cyclonic and anticyclonic domains. Primes here denote deviations from 31-day running mean. As seen in Chapter 5, maxima of V'V'300 locate in the eastern North Pacific for both cyclonic and anticyclonic domains, as the total Eulerian statistics. While the maximum value of the cyclonic V'V'300 shows only a hint of midwinter minimum, the anticyclonic V'V'300 shows its more distinct midwinter minimum, though the amplitude itself is weaker than the cyclonic counterpart. Lower-tropospheric meridional heat flux (V'T'850) from cyclonic domains is much larger than that from anticyclonic domains (Fig. A.4). The cyclonic contribution puts more emphasis on its spring peak with almost no signal of midwinter minimum, whereas the anticyclonic contribution shows its early-winter peak followed by a prominent midwinter minimum. These results are qualitatively very similar to those based on Lanczos filter with 8-day cutoff period shown in Chapter 5.

As in Chapter 5, we conduct energy budget analysis for eddy statistics based on 31-day running mean. The seasonal evolutions of EKE and EAPE for cyclones feature their weak

midwinter maximum (Fig. A.5a), while anticyclonic EKE and EAPE show distinct signals of midwinter minimum (Fig. A.5d), which is consistent with the more striking midwinter minimum of the Eulerian statistics for anticyclonic eddies (Fig. A.3). Figs. A.5b and A.5e show individual terms of energy conversion/generation separately for cyclones and anticyclones. Among the energy conversion/generation terms, CP and ET are much larger than the others. Cyclonic CP is larger than anticyclonic counterpart, consistent with the larger lower-tropospheric V'T' (Fig. A.4). Compared to the result based on the Lanczos filter with 8-day cutoff period (Fig. 5.42b), cyclonic CP shows a more prominent maximum in midwinter. To the contrary, anticyclonic CP still clearly shows a midwinter suppression. A striking difference from the result based on the Lanczos filter with 8-day cutoff period is found in CQ. CQ based on 31-day running mean, especially for cyclones, is distinctively negative in winter, while it is weakly positive in Chapter 5 with the Lanczos filter (Fig. 5.42b). Cyclonic and anticyclonic CQ associated only with precipitation are quite similar to that based on the Lanczos filter with 8-day cutoff period, indicating that sub-monthly low-frequency fluctuations of heat exchange with the ocean and radiative processes act as stronger damping. Cyclonic CK is less destructive in midwinter, which contrasts with the more destructive CK in midwinter based on the Lanczos filter with 8-day cutoff period.

As in Chapter 5, we calculate "efficiency" of the energy conversion/generation terms. The efficiency of CP is much larger than those of CK, CQ, and EF for cyclones and anticyclones (Fig. A.5c, f), showing that the baroclinic energy conversion is the most important maintenance mechanism among the processes associated with cyclones and anticyclones over the North Pacific even with eddy statistics based on the 31-day running

mean. A prominent midwinter maximum of net efficiency of cyclones is predominantly due to that of efficiency of CP. To the contrary, the efficiency of the net energy conversion/generation for anticyclonic eddies is clearly suppressed in midwinter, which is mainly contributed by the efficiency of CP.

From these results, the finding in the present study that anticyclones play a more important role in forming the midwinter minimum of the Eulerian statistics of migratory eddies along the North Pacific stormtrack is not qualitatively sensitive to the temporal filter utilized. Rather, the inclusion of sub-monthly low-frequency fluctuations makes the difference between cyclones and anticyclones more substantial.

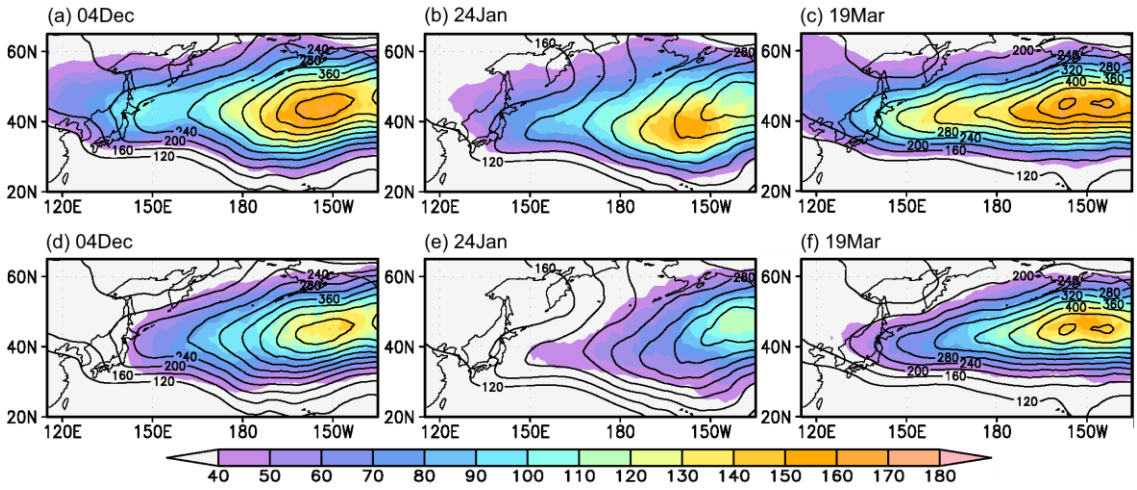

Figure A.3

(a-c) Climatological-mean V'V'300 (color, m^2/s^2) reconstructed only with cyclonic domains for the calendar days as indicated. Contours denote climatological-mean total V'V'300 (m^2/s^2). (d-f) Same as in (a-c), respectively, but for anticyclonic domains. Primes denote deviations from 31-day running mean.

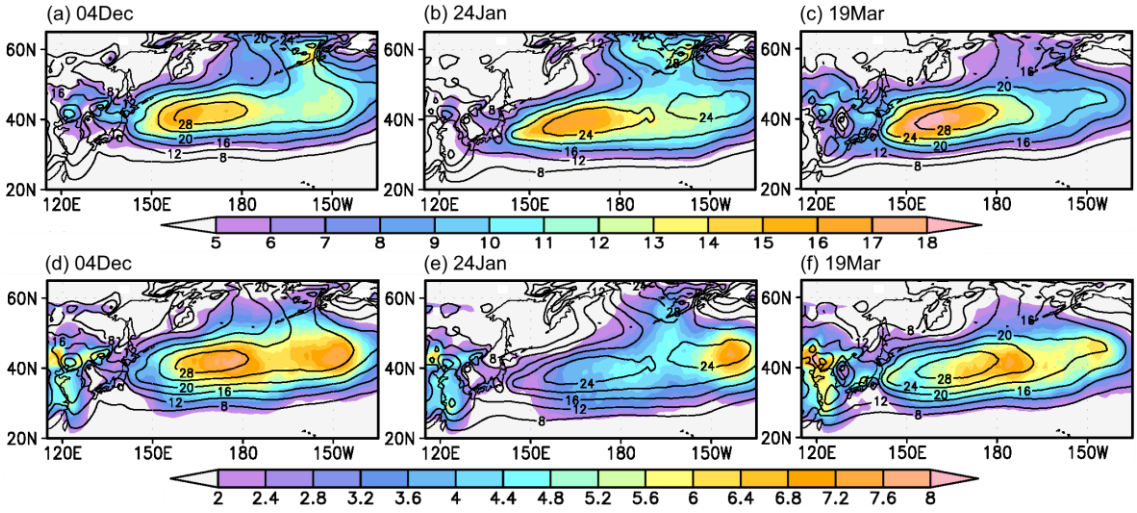

Figure A.4

Same as in Fig. A.3, but for V'T'850 (K m/s).

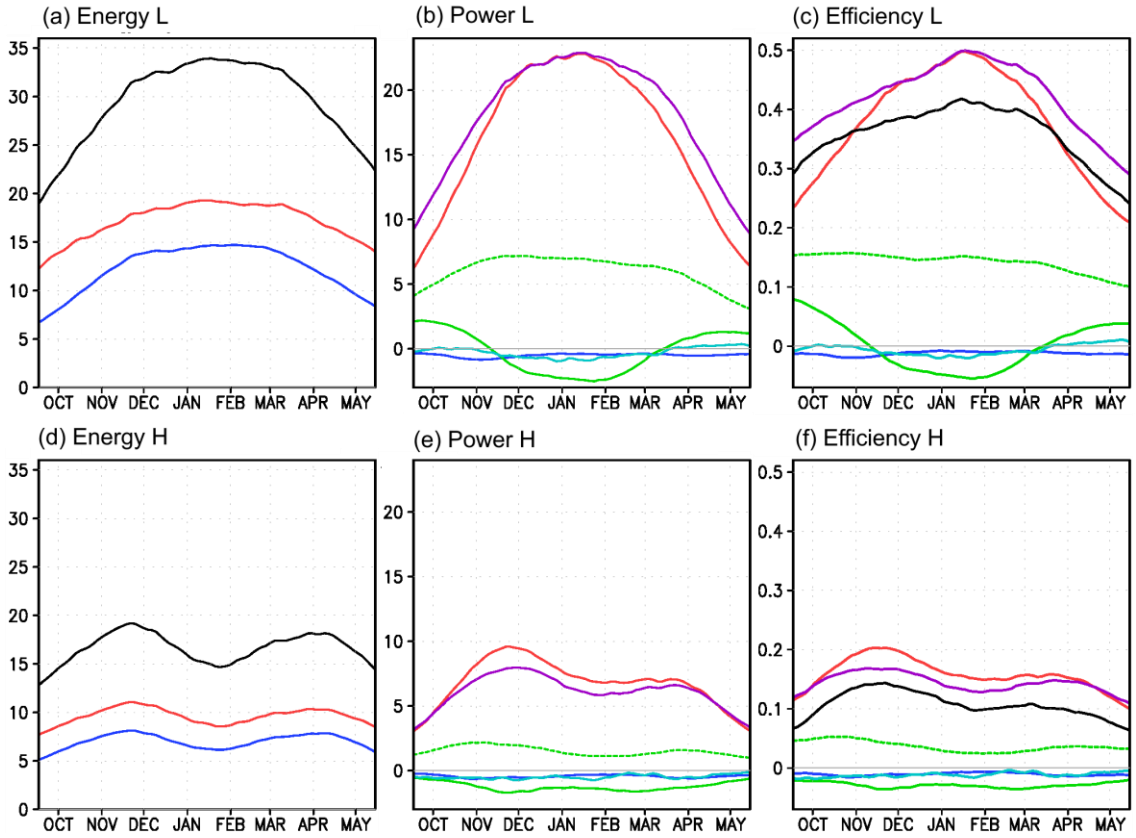

Figure A.5

(a) Climatological-mean seasonal evolution of EKE (blue), EAPE (red), and EKE+EAPE (black) for cyclonic domains, integrated three-dimensionally over the North Pacific (10^{19}J). (b) Same as in (a), but for power of CK (blue), CP (red), CQ (solid green), CQ associated only with precipitation (dotted green), EF (light blue), and ET (purple). Units are 10^{14}W. (c) Same as in (b), but for efficiency of CK (blue), CP (red), CQ (solid green), CQ associated only with precipitation (dotted green), EF (light blue), and ET (purple). Black line denotes total efficiency relevant to the budget of EKE+EAPE (namely, CK+CP+CQ+EF). Units are day^{-1}. (d-f) Same as in (a-c), respectively, but for anticyclonic domains. Eddy statistics are based on 31-day running mean.

Appendix C: Composite analysis only with stronger cyclones

In Chapter 5, we have constructed the composite maps of cyclones and anticyclones separately. All cyclones and anticyclones over a particular domain have been composited, but the numbers of the composited cyclones and anticyclones differs. As seen in Fig. 5.1, the density of cyclone centers is higher than the anticyclonic counterpart over the North Pacific. Actually, the number of composited cyclones is nearly three times as large as its anticyclonic counterpart in midwinter. We have conducted an additional composite analysis only with stronger cyclones to roughly equalize the number of composited cyclones and anticyclones. For this purpose, another condition is added for cyclones composited; maximum of ∇^2SLP near an identified cyclone center (see Section 2.3) must be stronger than 250 Pa/(100km)^2. Under this condition, the number of composited cyclones is nearly comparable to the anticyclonic counterpart during winter (44.10 and 35.49 on 24 Jan, and 40.03 and 49.87 on 04 Dec).

As plotted in Fig. A.6, the horizontal structure of the composited cyclone is qualitatively similar to that shown in Chapter 5. As expected, the amplitude of the composited cyclone becomes much larger, which is nearly comparable to that of the composited anticyclone in the upper troposphere. The composited surface cyclone is located on the northern flank of the low-level eddy-driven jet and accompanied by only a weak wave-like structure (Figs. A.6d-f). In the upper troposphere (Fig. A.6a-c), the cyclonic anomaly is located in the vicinity of the surface cyclone center, indicating that the cyclone vortex is not strongly baroclinic with weak tilting in the vertical. The upper-tropospheric anomaly is weaker than

that at the surface. In addition, the anomaly shows a midwinter minimum of its amplitude as in the composite for all cyclones (Fig. 5.12). The composited vertical structures are compared in Fig. A.7 between the strong cyclones and all the anticyclones. The composited cyclone (anticyclone) exhibits a vertically-tilted structure with a warm (cold) temperature anomaly ahead of the surface center, which is typical for baroclinic eddies. Still, the height anomalies associated with a surface cyclone tend to be more upright and more confined in the lower troposphere (Figs. A.7a-c), whereas the height anomalies associated with a surface anticyclone are deeper and more strongly tilted vertically (Figs. A.7d-f). As indicated in Fig. A.8, counterclockwise airflow is evident around the composited cyclone center. The southerly wind collocates with heavy precipitation accompanied by strong ascent just ahead of the center. The precipitation ahead of the center is heavier than its counterpart for all cyclones. It is stronger in early winter than the other seasons. Precipitation in the cold sector accompanied by a weak descent is confined in the lower troposphere and stronger in midwinter. The structure and seasonality of composite of stronger cyclones are qualitatively the same as those of all cyclones.

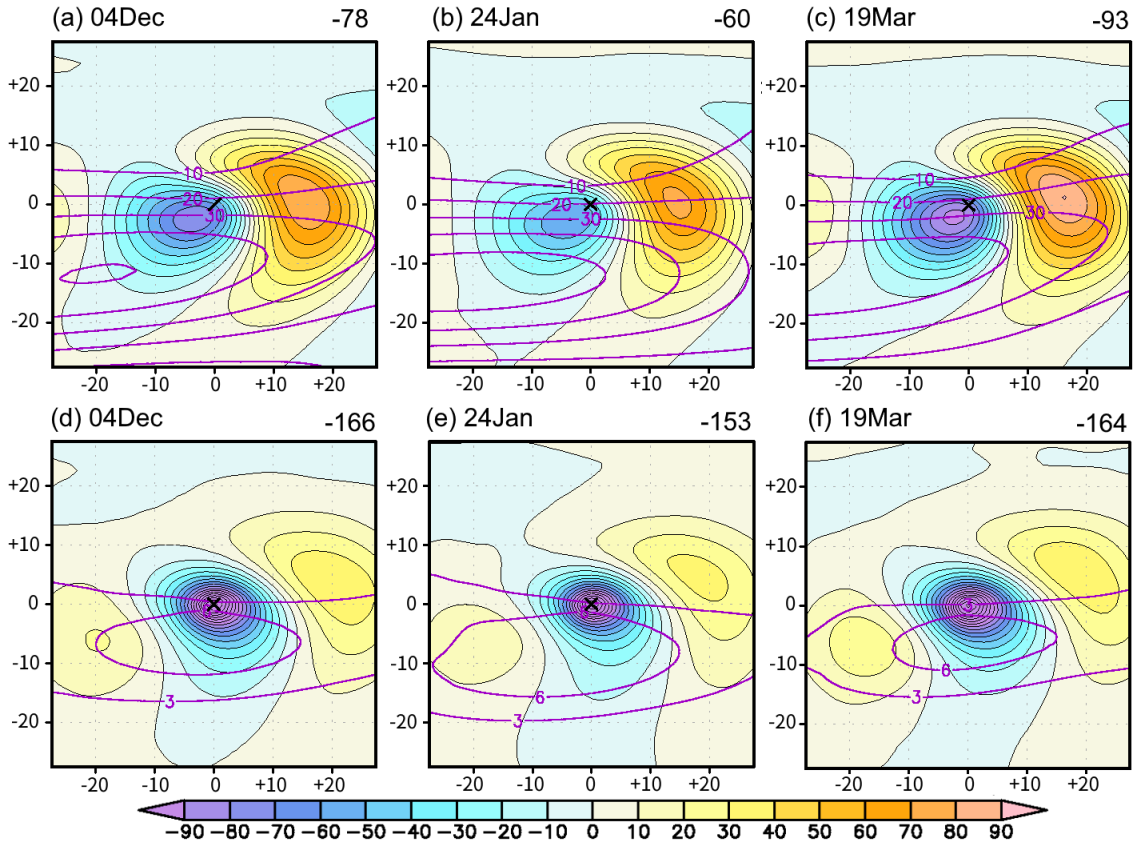

Figure A.6

Composited fields of highpass-filtered geopotential height (colors, m) at (a-c) 300-hPa and (d-f) 1000-hPa for centers of strong cyclones for the calendar days as indicated. Purple contours indicate composited lowpass-filtered westerly wind speed (m/s) at the respective levels. Numbers in the upper right denote height anomalies (m) at cyclone centers.

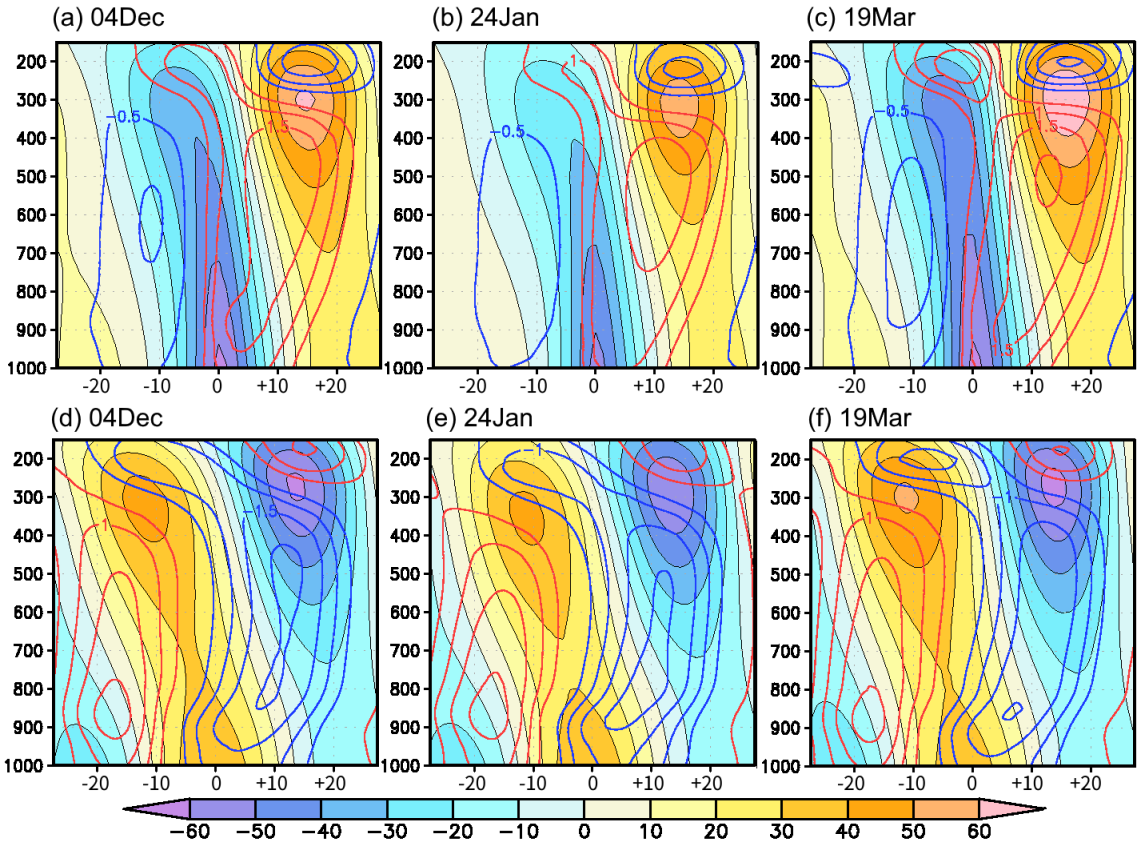

Figure A.7

Zonal sections of composited fields of highpass-filtered geopotential height (colors, m) and temperature (colored contours, K) for (a-c) strong cyclones and (d-f) all anticyclones for the calendar days as indicated. Quantities plotted are averaged within the 20° latitudinal bands centered at the surface centers. Panels of (d-f) are identical to Figs. 5.14d-f.

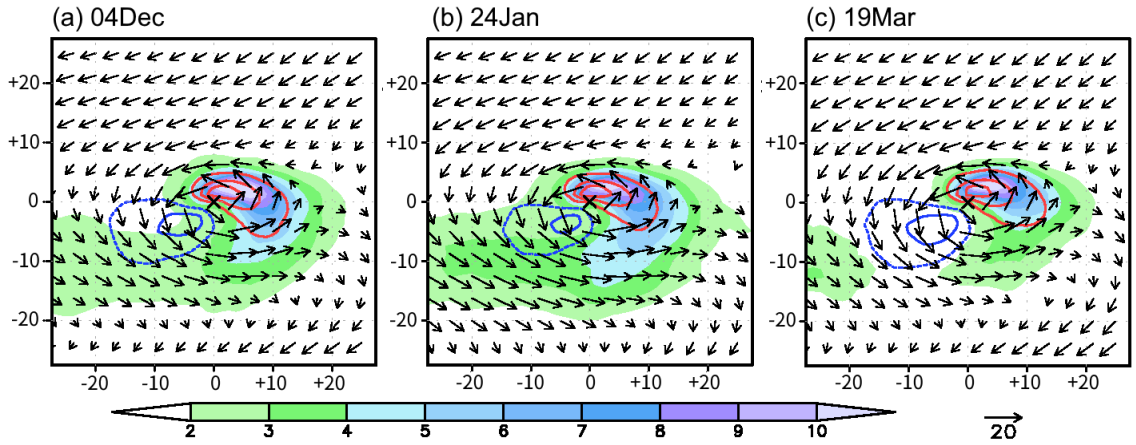

Figure A.8

Same as in Fig. A.6, but for diabatic heating rate associated only with precipitation (colors, K/day), winds relative to the movement of surface centers (vector, m/s), and vertical motion (red contours for upward and blue for downward, every 10hPa/h and zero contours are omitted) all at 700-hPa. Dashed blue contours denote 5hPa/h.

Acknowledgments

I am most grateful to Prof. H. Nakamura for his guidance and ceaseless encouragement throughout the course of this study. Valuable comments and suggestions from the member of the dissertation committee, Profs. M. Watanabe, Y. Masumoto, K. Iga, and H. Miura were also grateful. I appreciate Dr. T. Miyasaka for providing me fruitful comments and a program to evaluate eddy feedback forcing. I also appreciate valuable comments and advises by Dr. Y. Kosaka, Dr. M. Mori, Prof. B. Taguchi, Dr. P. Martineu, and Dr. L. Robert. I also thank Prof. Y. Kaspi for fruitful discussion. I also appreciate all the students of our research group for creating a cheerful atmosphere. Finally, I wish to express my appreciation to my family for their understanding and kind support.

References

Afargan, H. and Y. Kaspi, 2017: A midwinter minimum in North Atlantic storm track intensity in years of a strong jet. *Geophysical Research Letters*, **44(24)**, 12-511.

Akahori, K. and S. Yoden, 1997: Zonal flow vacillation and bimodality of baroclinic eddy life cycles in a simple global circulation model. *Journal of the atmospheric sciences*, **54(19)**, 2349-2361.

Bell, G. D. and L. F. Bosart, 1989: A 15-year climatology of Northern Hemisphere 500 mb closed cyclone and anticyclone centers. *Monthly Weather Review*, **117(10)**, 2142-2164.

Blackmon, M. L., 1976: A climatological spectral study of the 500 mb geopotential height of the Northern Hemisphere. *Journal of the Atmospheric Sciences*, **33(8)**, 1607-1623.

Blackmon, M. L., J. M. Wallace, N. C. Lau, and S. L. Mullen, 1977: An observational study of the Northern Hemisphere wintertime circulation. *Journal of the Atmospheric Sciences*, **34(7)**, 1040-1053.

Browning, K. A., 1997: The dry intrusion perspective of extra-tropical cyclone development. *Meteorological Applications*, **4(4)**, 317-324.

Carlson, T. N., 1980: Airflow through midlatitude cyclones and the comma cloud pattern. Monthly Weather Review, **108(10)**, 1498-1509.

Catto, J. L., L. C. Shaffrey, and K. I. Hodges, 2010: Can climate models capture the structure of extratropical cyclones?. *Journal of Climate*, **23(7)**, 1621-1635.

Catto, J. L. and S. Pfahl, 2013: The importance of fronts for extreme precipitation. *Journal of Geophysical Research: Atmospheres*, **118(19)**, 10-791.

Chang, E. K., 1993: Downstream development of baroclinic waves as inferred from regression analysis. *Journal of the atmospheric sciences*, **50(13)**, 2038-2053.

Chang, E. K., 2001: GCM and observational diagnoses of the seasonal and interannual variations of the Pacific storm track during the cool season. *Journal of the atmospheric sciences*, **58(13)**, 1784-1800.

Chang, E. K., S. Lee, and K. L. Swanson, 2002: Storm track dynamics. *Journal of climate*, **15(16)**, 2163-2183.

Chang, E. K., 2005: The impact of wave packets propagating across Asia on Pacific cyclone development. *Monthly weather review*, **133(7)**, 1998-2015.

Chang, E. K. and S. Song, 2006: The seasonal cycles in the distribution of precipitation around cyclones in the western North Pacific and Atlantic. *Journal of the atmospheric sciences*, **63(3)**, 815-839.

Chang, E. K. and Y. Guo, 2012: Is Pacific storm-track activity correlated with the strength of upstream wave seeding?, *Journal of Climate*, **25(17)**, 5768-5776.

Chang, E. K., Y. Guo, Y., and X. Xia, 2012: CMIP5 multimodel ensemble projection of storm track change under global warming. *Journal of Geophysical Research: Atmospheres*, **117**, D23118.

Chelton, D. B., M. G. Schlax, M. G., and R. M. Samelson, 2011: Global observations of nonlinear mesoscale eddies. *Progress in Oceanography*, **91(2)**, 167-216.

Chen, S. J., Y. H. Kuo, P. Z. Zhang, and Q. F. Bai, 1991: Synoptic climatology of cyclogenesis over East Asia, 1958-1987. *Monthly Weather Review*, **119(6)**, 1407-1418.

Christoph, M., U. Ulbrich, and P. Speth, 1997: Midwinter suppression of Northern Hemisphere storm track activity in the real atmosphere and in GCM experiments. *Journal of the atmospheric sciences*, **54(12)**, 1589-1599.

Dee, D. P., and coauthors 2011: The ERA-Interim reanalysis: Configuration and performance of the data assimilation system. *Quarterly Journal of the royal meteorological society*, **137(656)**, 553-597.

Deng, Y. and M. Mak, 2005: An idealized model study relevant to the dynamics of the midwinter minimum of the Pacific storm track. *Journal of the atmospheric sciences*, **62(4)**, 1209-1225.

Deng, Y. and M. Mak, 2006: Nature of the differences in the intraseasonal variability of the Pacific and Atlantic storm tracks: A diagnostic study. *Journal of the atmospheric*

sciences, **63(10)**, 2602-2615.

Eady, E. T., 1949: Long waves and cyclone waves. *Tellus*, **1(3)**, 33-52.

Favre, A. and A. Gershunov, 2006: Extra-tropical cyclonic/anticyclonic activity in North-Eastern Pacific and air temperature extremes in Western North America. *Climate Dynamics*, **26(6)**, 617-629.

Garfinkel, C. I. and D. W. Waugh, 2014: Tropospheric Rossby wave breaking and variability of the latitude of the eddy-driven jet. *Journal of Climate*, **27(18)**, 7069-7085.

Gyakum, J. R., J. R. Anderson, R. H. Grumm, and E. L. Gruner, 1989: North Pacific cold-season surface cyclone activity: 1975–1983. *Monthly weather review*, **117(6)**, 1141-1155.

Harada, Y., H. Kamahori, C. Kobayashi, H. Endo, S. Kobayashi, Y. Ota, H. Onoda, K. Onogi, K. Miyaoka, and K. Takahashi, 2016: The JRA-55 Reanalysis: Representation of atmospheric circulation and climate variability, *J. Meteor. Soc. Japan*, **94**, 269-302.

Harnik, N. and E. K. Chang, 2004: The effects of variations in jet width on the growth of baroclinic waves: Implications for midwinter Pacific storm track variability. *Journal of the atmospheric sciences*, **61(1)**, 23-40.

Harrold, T. W., 1973: Mechanisms influencing the distribution of precipitation within baroclinic disturbances. *Quarterly Journal of the Royal Meteorological Society*, **99(420)**, 232-251.

Hartmann, D. L. and P. Zuercher, 1998: Response of baroclinic life cycles to barotropic shear. *Journal of the atmospheric sciences*, **55(3)**, 297-313.

Hinman, R., 1888: *Eclectic physical geography*. American Book Company.

Hirata, H., R. Kawamura, M. Kato, and T. Shinoda, 2015: Influential role of moisture supply from the Kuroshio/Kuroshio Extension in the rapid development of an extratropical cyclone. *Monthly Weather Review*, **143(10)**, 4126-4144.

Hodges, K. I., 1994: A general method for tracking analysis and its application to

meteorological data. Monthly Weather Review, **122(11)**, 2573-2586.

Hodges, K. I., 1995: Feature tracking on the unit sphere. *Monthly Weather Review*, **123(12)**, 3458-3465.

Hodges, K. I., 1999: Adaptive constraints for feature tracking. *Monthly Weather Review*, **127(6)**, 1362-1373.

Holton, J. R., 2004; An introduction to dynamic meteorology, 4th edition.

Hoskins, B. J., I. N. James, and G. H. White, 1983: The shape, propagation and mean-flow interaction of large-scale weather systems. *J. Atmos. Sci.*, **40**, 1595–1612.

Hoskins, B. J. and K. I. Hodges, 2002: New perspectives on the Northern Hemisphere winter storm tracks. *Journal of the Atmospheric Sciences*, **59(6)**, 1041-1061.

Hoskins, B. J. and K. I. Hodges, 2019: The annual cycle of Northern Hemisphere storm tracks. Part I: Seasons. *Journal of Climate*, **32(6)**, 1743-1760.

Hoskins, B. J. and K. I. Hodges, 2019: The annual cycle of Northern Hemisphere storm tracks. Part II: Regional detail. *Journal of Climate*, **32(6)**, 1761-1775.

Hotta, D., and H. Nakamura, 2011: On the significance of the sensible heat supply from the ocean in the maintenance of the mean baroclinicity along storm tracks. *Journal of Climate*, **24(13)**, 3377-3401.

Hurrell, J. W., 1995: Transient eddy forcing of the rotational flow during northern winter. *Journal of the atmospheric sciences*, **52(12)**, 2286-2301.

James, I. N., 1987: Suppression of baroclinic instability in horizontally sheared flows. *Journal of the atmospheric sciences*, **44(24)**, 3710-3720.

Kelly, K. A., R. J. Small, R. M. Samelson, B. Qiu, T. M. Joyce, Y. O. Kwon, and M. F. Cronin, 2010: Western boundary currents and frontal air–sea interaction: Gulf Stream and Kuroshio Extension. *Journal of Climate*, **23(21)**, 5644-5667.

Klein, W. H., 1958: The frequency of cyclones and anticyclones in relation to the mean circulation. *Journal of Meteorology*, **15(1)**, 98-102.

Kobayashi, S., Y. Ota, Y. Harada, A. Ebita, M. Moriya, H. Onoda, K. Onogi, H. Kamahori,

C. Kobayashi, H. Endo, K. Miyaoka, and K. Takahashi, 2015: The JRA-55 Reanalysis: General specifications and basic characteristics. *J. Meteor. Soc. Japan*, **93**, 5-48.

Kravtsov, S., I. Rudeva, and S. K. Gulev, 2015: Reconstructing sea level pressure variability via a feature tracking approach. *Journal of the Atmospheric Sciences*, **72(1)**, 487-506.

Lachmy, O. and N. Harnik, 2014: The transition to a subtropical jet regime and its maintenance. *Journal of the Atmospheric Sciences*, **71(4)**, 1389-1409.

Lachmy, O. and N. Harnik, 2016: Wave and jet maintenance in different flow regimes. *Journal of the Atmospheric Sciences*, **73(6)**, 2465-2484.

Lachmy, O. and N. Harnik, 2019: Tropospheric Jet Variability in Different Flow Regimes. *Quarterly Journal of the Royal Meteorological Society, in press*.

Landsberg, H., J. M. Mitchell Jr, and H. Crutcher, 1959: Power Spectrum Analysis of Climatological Data for Woodstock College, Maryland. *Monthly Weather Review*, **87(8)**, 283-298.

Lau, N.-C. and E. O. Holopainen, 1984: Transient eddy forcing of the time-mean flow as identified by geopotential tendencies. *J. Atmos. Sci.*, **41**, 313–328.

Lee, S. S., J. Y. Lee, K. J. Ha, B. Wang, A. Kitoh, Y. Kajikawa, and M. Abe, 2013: Role of the Tibetan Plateau on the annual variation of mean atmospheric circulation and storm-track activity. *Journal of Climate*, **26(14)**, 5270-5286.

Lefevre, R. J. and J. W. Nielsen-Gammon, 1995: An objective climatology of mobile troughs in the Northern Hemisphere. *Tellus A*, **47(5)**, 638-655.

Lorenz, E. N., 1955: Available potential energy and the maintenance of the general circulation. *Tellus*, **7(2)**, 157-167.

Lorenz, D. J. and D. L. Hartmann, 2001: Eddy–zonal flow feedback in the Southern Hemisphere. *Journal of the atmospheric sciences*, **58(21)**, 3312-3327.

Madonna, E., C. Li, and J. J. Wettstein, 2019: Suppressed eddy driving during southward excursions of the North Atlantic jet on synoptic to seasonal time scales. *Atmospheric*

Science Letters, in press.

Manobianco, J., 1989: Explosive east coast cyclogenesis over the west-central North Atlantic Ocean: A composite study derived from ECMWF operational analyses. *Monthly Weather Review*, **117(11)**, 2365-2383.

Masunaga, R., H. Nakamura, B. Taguchi, and T. Miyasaka, 2020: Processes Shaping the Frontal-Scale Time-Mean Surface Wind Convergence Patterns around the Kuroshio Extension in Winter. *Journal of Climate*, **33(1)**, 3-25.

Murray, R. J. and I. Simmonds, 1991: A numerical scheme for tracking cyclone centres from digital data. Part II: Application to January and July general circulation model simulations. *Australian Meteorological Magazine*, **39(3)**, 167-180.

Nakamura, H., 1992: Midwinter suppression of baroclinic wave activity in the Pacific. *Journal of the Atmospheric Sciences*, **49(17)**, 1629-1642.

Nakamura, H., and J. M. Wallace, 1993: Synoptic behavior of baroclinic eddies during the blocking onset. *Monthly weather review*, **121(7)**, 1892-1903.

Nakamura, H., M. Nakamura, J. L. Anderson, 1997: The role of high-and low-frequency dynamics in blocking formation. *Monthly Weather Review*, **125(9)**, 2074-2093.

Nakamura, H. and T. Sampe, 2002: Trapping of synoptic-scale disturbances into the North-Pacific subtropical jet core in midwinter. *Geophysical Research Letters*, **29(16)**, 8-1.

Nakamura, H., T. Izumi, and T. Sampe, 2002: Interannual and decadal modulations recently observed in the Pacific storm track activity and East Asian winter monsoon. *Journal of Climate*, **15(14)**, 1855-1874.

Nakamura, H., T. Sampe, Y. Tanimoto, and A. Shimpo, 2004: Observed associations among storm tracks, jet streams, and midlatitude oceanic fronts. *Earth Climate: The Ocean–Atmosphere Interaction*, *Geophys. Monogr.*, **147**, Amer. Geophys. Union, 329–345.

Nakamura, H., T. Miyasaka, Y. Kosaka, K. Takaya, and M. Honda, 2010: Northern Hemisphere extratropical tropospheric planetary waves and their low-frequency variability: Their vertical structure and interaction with transient eddies and surface

thermal contrasts. *Climate dynamics: why does climate vary*, **189**, 149-79.

Neu, U., and coauthors, 2013: IMILAST: A community effort to intercompare extratropical cyclone detection and tracking algorithms. *Bulletin of the American Meteorological Society*, **94(4)**, 529-547.

Nishii, K., H. Nakamura, and T. Miyasaka, 2009: Modulations in the planetary wave field induced by upward propagating Rossby wave packets prior to stratospheric sudden warming events: A case study. *Quarterly Journal of the Royal Meteorological Society*, **135(638)**, 39-52.

Novak, L., T. Schneider, and F. Ait-Chaalal, 2020: Midwinter suppression of storm tracks in an idealized zonally symmetric setting. *Journal of the Atmospheric Sciences*, **77(1)**, 297-313.

Okajima, S., H. Nakamura, K. Nishii, T. Miyasaka, A. Kuwano-Yoshida, B. Taguchi, M. Mori, and Y. Kosaka, 2018: Mechanisms for the maintenance of the wintertime basin-scale atmospheric response to decadal SST variability in the North Pacific subarctic frontal zone. *Journal of Climate*, **31(1)**, 297-315.

Okubo, A., 1970: Horizontal dispersion of floatable particles in the vicinity of velocity singularities such as convergences. *Deep sea research and oceanographic abstracts*, **17(3)**, 445-454.

Orlanski, I. and J. Katzfey, 1991: The life cycle of a cyclone wave in the Southern Hemisphere. Part I: Eddy energy budget. *Journal of the Atmospheric Sciences*, **48(17)**, 1972-1998.

Park, H. S., J. C. Chiang, and S. W. Son, 2010: The role of the central Asian mountains on the midwinter suppression of North Pacific storminess. *Journal of the Atmospheric Sciences*, **67(11)**, 3706-3720.

Parker, S. S., J. T. Hawes, S. J. Colucci, and B. P. Hayden, 1989: Climatology of 500 mb cyclones and anticyclones, 1950–85. *Monthly weather review*, **117(3)**, 558-571.

Penny, S., G. H. Roe, and D. S. Battisti, 2010: The source of the midwinter suppression in storminess over the North Pacific. *Journal of Climate*, **23(3)**, 634-648.

Penny, S. M., D. S. Battisti, and G. H. Roe, 2013: Examining mechanisms of variability within the Pacific storm track: Upstream seeding and jet-core strength. *Journal of Climate*, **26(14)**, 5242-5259.

Pfahl, S., E. Madonna, M. Boettcher, H. Joos, and H. Wernli, 2014: Warm conveyor belts in the ERA-Interim dataset (1979–2010). Part II: Moisture origin and relevance for precipitation. *Journal of Climate*, **27(1)**, 27-40.

Piva, E. D., M. A. Gan, and V. B. Rao, 2008: An objective study of 500-hPa moving troughs in the Southern Hemisphere. *Monthly Weather Review*, **136(6)**, 2186-2200.

Plumb, R. A., 1986: Three-dimensional propagation of transient quasi-geostrophic eddies and its relationship with the eddy forcing of the time—mean flow. *Journal of the atmospheric sciences*, **43(16)**, 1657-1678.

Robert, L., G. Rivière, and F. Codron, 2017: Positive and negative eddy feedbacks acting on midlatitude jet variability in a three-level quasigeostrophic model. *Journal of the Atmospheric Sciences*, **74(5)**, 1635-1649.

Rogers, J. C., 1997: North Atlantic storm track variability and its association to the North Atlantic Oscillation and climate variability of northern Europe. *Journal of Climate*, **10(7)**, 1635-1647.

Sawyer, J. S., 1970: Observational characteristics of atmospheric fluctuations with a time scale of a month. *Quarterly Journal of the Royal Meteorological Society*, **96(410)**, 610-625.

Schemm, S. and T. Schneider, 2018: Eddy lifetime, number, and diffusivity and the suppression of eddy kinetic energy in midwinter. *Journal of Climate*, **31(14)**, 5649-5665.

Schemm, S. and G. Rivière, 2019. On the Efficiency of Baroclinic Eddy Growth and how it Reduces the North Pacific Storm Track Intensity in Midwinter. *Journal of Climate*, **32(23)**, 8373-8398.

Shapiro, M. A., and D. Keyser, 1990: Fronts, jet streams and the tropopause. *Extratropical Cyclones: The Erik Palmén Memorial Volume*, C. W. Newton and E. O. Holopainen, Eds., Amer. Meteor. Soc., 167–191.

Shaw, T. A. and coauthors, 2016: Storm track processes and the opposing influences of climate change. *Nature Geoscience*, **9(9)**, 656.

Simmons, A. J., J. M. Wallace, and G. W. Branstator, 1983: Barotropic wave propagation and instability, and atmospheric teleconnection patterns. *J. Atmos. Sci.*, **40,** 1363–1392.

Sinclair, M. R., 1994: An objective cyclone climatology for the Southern Hemisphere. *Monthly Weather Review*, **122(10)**, 2239-2256.

Takano, I., 2002: Analysis of an intense winter extratropical cyclone that advanced along the south coast of Japan. *Journal of the Meteorological Society of Japan. Ser. II*, **80(4)**, 669-695.

Takaya, K. and H. Nakamura, 1997: A formulation of a wave-activity flux for stationary Rossby waves on a zonally varying basic flow. Geophysical research letters, **24(23)**, 2985-2988.

Takaya, K. and H. Nakamura, 2001: A formulation of a phase-independent wave-activity flux for stationary and migratory quasigeostrophic eddies on a zonally varying basic flow. *J. Atmos. Sci*., **58**, 608-627.

Takaya, K. and H. Nakamura, 2005: Geographical dependence of upper-level blocking formation associated with intraseasonal amplification of the Siberian high. *Journal of the atmospheric sciences*, **62(12)**, 4441-4449.

Tamarin, T. and Y. Kaspi, 2016: The poleward motion of extratropical cyclones from a potential vorticity tendency analysis. *Journal of the Atmospheric Sciences*, **73(4)**, 1687-1707.

Thompson, D. W., and J. M. Wallace, 2000: Annular modes in the extratropical circulation. Part I: Month-to-month variability. *Journal of climate*, **13(5)**, 1000-1016.

Thompson, D. W., and J. D. Woodworth, 2014: Barotropic and baroclinic annular variability in the Southern Hemisphere. *Journal of the Atmospheric Sciences*, **71(4)**, 1480-1493.

Thorncroft, C. D., B. J. Hoskins, and M. E. McIntyre, 1993: Two paradigms of baroclinic-

wave life-cycle behaviour. *Quarterly Journal of the Royal Meteorological Society*, **119(509)**, 17-55.

Trenberth, K. E., 1986: An assessment of the impact of transient eddies on the zonal flow during a blocking episode using localized Eliassen-Palm flux diagnostics. *J. Atmos. Sci.*, **43**, 2070–2087.

Ulbrich, U., J. G. Pinto, H. Kupfer, G. C. Leckebusch, T. Spangehl, and M. Reyers, 2008: Changing Northern Hemisphere storm tracks in an ensemble of IPCC climate change simulations. *Journal of climate*, **21(8)**, 1669-1679.

Ulbrich, U., G. C. Leckebusch, and J. G. Pinto, 2009: Extra-tropical cyclones in the present and future climate: a review. *Theoretical and Applied Climatology*, **96(1-2)**, 117-131.

Viúdez, Á. and R. L. Haney, 1996: On the shear and curvature vorticity equations. Journal of the atmospheric sciences, **53(22)**, 3384-3394.

Wallace, J. M., G. H. Lim, and M. L. Blackmon, 1988: Relationship between cyclone tracks, anticyclone tracks and baroclinic waveguides. *Journal of the atmospheric sciences*, **45(3)**, 439-462.

Wang, C. C. and J. C. Rogers, 2001: A composite study of explosive cyclogenesis in different sectors of the North Atlantic. Part I: Cyclone structure and evolution. *Monthly Weather Review*, **129(6)**, 1481-1499.

Weiss, J., 1991: The dynamics of enstrophy transfer in two-dimensional hydrodynamics. *Physica D: Nonlinear Phenomena*, **48(2-3)**, 273-294.

Wernli, H. and L. Papritz, 2018: Role of polar anticyclones and mid-latitude cyclones for Arctic summertime sea-ice melting. *Nature Geoscience*, **11(2)**, 108.

Whittaker, L. M. and L. H. Horn, 1984: Northern Hemisphere extratropical cyclone activity for four mid-season months. *Journal of Climatology*, **4(3)**, 297-310.

Whitaker, J. S. and P. D. Sardeshmukh, 1998: A linear theory of extratropical synoptic eddy statistics. *Journal of the atmospheric sciences*, **55(2)**, 237-258.

Yin, J. H., 2005: A consistent poleward shift of the storm tracks in simulations of 21st century climate. *Geophysical Research Letters*, **32(18)**, L18701.

Yuval, J. and Y. Kaspi, 2018: Eddy sensitivity to jet characteristics. *Journal of the Atmospheric Sciences*, **75(5)**, 1371-1383.

Yuval, J. H. Afargan, and Y. Kaspi, 2018: The relation between the seasonal changes in jet characteristics and the Pacific Midwinter Minimum in eddy activity. *Geophysical Research Letters*, **45(18)**, 9995-10002.

Zhao, Y. and X. S. Liang, 2019: Causes and underlying dynamic processes of the mid-winter suppression in the North Pacific storm track. *Science China Earth Sciences*, **62(5)**, 872-890.

Zhang, Y. and I. M. Held, 1999: A linear stochastic model of a GCM's midlatitude storm tracks. *Journal of the atmospheric sciences*, **56(19)**, 3416-3435.